Application of Modified Smooth Exterior Scaling Method to Study Auger and Shape Resonances in Different Atomic and Molecular Systems

A thesis submitted to

Indian Institute of Technology Guwahati

for the award of the degree of

Doctor of Philosophy

by

Mwdansar Banuary

(Roll No. 166122103)

Under the Guidance of

Prof. Ashish Kumar Gupta

Department of Chemistry

Indian Institute of Technology Guwahati

Guwahati-781039, Assam, India

Certificate

This is to certify that the thesis entitled **"Application of Modified Smooth Exterior Scaling Method to Study Auger and Shape Resonances in Different Atomic and Molecular Systems"**, submitted by **Mwdansar Banuary** to the Indian Institute of Technology Guwahati, for the award of the degree of **Doctor of Philosophy (Ph.D.)** in Chemistry, is a record of the original, bona fide research work carried out by him under my supervision and guidance. The thesis has reached the standards fulfilling the requirements of the regulations related to the award of the degree.

The results contained in this thesis have not been submitted in part or in full to any other University or Institute for the award of any degree or diploma to the best of our knowledge.

Prof. Ashish Kumar Gupta
Department of Chemistry
Indian Institute of Technology Guwahati
Guwahati-781039, India

Declaration

I declare that the thesis entitled **"Application of Modified Smooth Exterior Scaling Method to Study Auger and Shape Resonances in Different Atomic and Molecular Systems"** submitted by me to the Indian Institute of Technology Guwahati for the award of Doctor of Philosophy is the record of research work carried out by me under the guidance of **Prof. Ashish Kumar Gupta** and written in my own words. Where others' ideas and words have been included, I have adequately cited and referenced the original source. This work has not been submitted elsewhere for the award of any degree or diploma.

Mwdansar Banuary
Roll No.: 166122103
IIT Guwahati, India

Dedicated to my beloved Grandmother and Parents.

Acknowledgments

First of all, I would like to thank my advisor, ***Prof. Ashish Kumar Gupta***, for his constant help and support during my career as a graduate student and researcher. Had he not been there to help me with my small and not–so–small problems in every wake of my research none of the work presented here would have taken shape. His knowledge, wisdom, and experience have always been a source of inspiration for me.

I would like to thank all my Doctoral Committee members: ***Prof. Sumana Dutta***, ***Prof. Aditya Narayan Panda***, and ***Dr. Manabendra Sarma*** for their constant support and valuable pieces of advice.

I am thankful to IIT Guwahati for providing PARAM-ISHAN and PARAM-KAMRUPA supercomputing facilities. I also acknowledge the IIT Guwahati for financial support.

I thank my lab mates Sayantani, Deepak, and Rolly for the pleasant atmosphere they created during work-time and for various kinds of help in research works.

I am thankful to all my school, college, university, and IITG friends. I feel myself very lucky as I enjoyed my PhD journey with Nerswn, Srimanta, Himangshu, Haobam, Rabindranath, Deepak, Shubham, and Palak.

I would also like to thank my parents for their unconditional love and care and for being there for me at every stage of my life.

I take the opportunity to thank my parents–in–law as well, who have always been a constant source of love, support, and motivation.

Thanks go to Dr. Dhruba Jyoti Kalita too, on whose recommendation I got the chance to work in this Lab.

Last, but not least, I would like to thank my lovely wife, Ms. Dipa Basumatary for being at my side always and motivating me all the way along.

Mwdansar Banuary

Contents

List of Figures

List of Tables

Abbreviations

LEEs	**L**ow **E**nergy **E**lectrons
TDSE	**T**ime **D**ependent **S**chrodinger **E**quation
TISE	**T**ime **I**ndependent **S**chrodinger **E**quation
CS	**C**omplex **S**caling
SCF	**S**elf **C**onsistent **F**ield
MCSFC	**M**ulti **C**onfigurational **S**elf **C**onsistent **F**ield
DFT	**D**ensity **F**unctional **T**heory
ECS	**E**xterior **C**omplex **S**caling
CBFs	**C**omplex **B**asis **F**unctions
CAP	**C**omplex **A**bsorbing **P**otential
RF-CAP	**R**eflection **F**ree **C**omplex **A**bsorbing **P**otential
SES	**S**mooth **E**xterior **S**caling
MSES	**M**odified **S**mooth **E**xterior **S**caling
CSES	**C**onventional **S**mooth **E**xterior **S**caling
IP	**I**onization **P**otential
EA	**E**lectron **A**ffinity
ZoDEP	**Z**eroth **O**rder **D**ilated **E**lectron **P**ropagator
ZoDEP-MSES	**Z**eroth **O**rder **D**ilated **E**lectron **P**ropagator **M**odified **S**mooth **E**xterior **S**caling
SCF-MSES	**S**elf **C**onsistent **F**ield **M**odified **S**mooth **E**xterior **S**caling
SoDEP-MSES	**S**econd **O**rder **D**ilated **E**lectron **P**ropagator **M**odified **S**mooth **E**xterior **S**caling
ToDEP-MSES	**T**hird **O**rder **D**ilated **E**lectron **P**ropagator **M**odified **S**mooth **E**xterior **S**caling
LUMO	**L**owest **U**noccupied **M**olecular **O**rbital

Symbols

ψ	psi
$\hbar$	Planck's Constant
Γ	Gamma
τ	tau
Ψ	Psi
μ	mu
∞	infinity
α	alpha
θ	theta
η	eta
δ	delta
∇	Del
π	pi
Π	Pi
∂	partial derivative
λ	lambda
σ	sigma
Σ	Sigma
$\dagger$	dagger
ϕ	phi
Φ	Phi
ω	omega
$\int$	integral
ρ	rho
ϵ	epsilon
Å	Angstrom

$\star$	asterisk
ν	nu

Abstract

Resonances are the results of electron-atom or electron-molecule scattering experiments. These are exponentially decaying long-lived metastable states of a system that can break up into several subsystems as time elapses. Generally, resonances can be obtained as the complex eigenvalues, $E_{res} = E_R - i\frac{\Gamma}{2}$ by solving the time-independent Schrödinger equation (TISE), $H\psi = E\psi$, where the Hamiltonian is non-Hermitian. E_R of the complex eigenvalue represents the resonance position and Γ represents the width of resonance which is inversely related to lifetime by the relation $\tau = \frac{\hbar}{\Gamma}$. The corresponding wave functions, called Siegert wave functions, diverge asymptotically and are not square integrable which makes it difficult in calculating by using standard electronic structure techniques. The basic idea behind converting the divergent wave function into a bounded normalizable function is carrying out a suitable mathematical transformation. By this way, wave functions become a part of Hilbert space. Among the various approaches, complex scaling (CS) and complex absorbing potential (CAP) are the most extensively used approaches for this purpose.

Due to some limitations in CS and CAP techniques, an alternative method called the smooth exterior scaling (SES) method was developed. SES is an efficient method based on the rigorous mathematical theory of CS and shares the property of CAP in its application. A method called modified smooth exterior scaling (MSES) was proposed and successfully applied to a time-dependent dynamics problem. The MSES is a modified version of the SES method. The fundamental difference between MSES and SES is the scaling function $\theta(x) = \theta_0 a(x)$ is chosen as real in MSES which is complex in SES. The scaling by the MSES method has been reported to be much smoother and displays efficient absorption during wavepacket propagation at the grid boundary.

The dilated Hamiltonian (complex scaled) produced by using any of the above mentioned analytical continuation methods becomes non-Hermitian but remains complex symmetric. Therefore, the conventional self-consistent field (SCF) method becomes inapplicable to solve the problem. In this case, the resonant eigenvalues can be obtained by applying bivariational SCF method.

The electron propagator theory has been a powerful and effective tool for the direct calculation of electron detachment and electron attachment energies. The dilated

electron propagator (complex scaled) is a convenient method to calculate the energies and width of resonances directly from the electron attachment energy (shape resonance) and electron removal energy (Auger resonance) of the metastable state. Further, these energies can be improved by using higher order perturbative decouplings of dilated electron propagator incorporating a greater extent of relaxation and correlation effects.

The main objective of our work is to formulate the MSES method in bivariational SCF and electron propagator methods. We have applied the dilated electron propagator up to the second order in the case of molecular systems and up to the third order in the case of atomic systems. The shape resonances of isoelectronic systems $^2\Pi_g$ N_2^- and $^2\Pi$ CO^- are studied. In this study, MSES is used for the first time in electronic structure calculation. The dilated electron propagator method is also used up to the second order to include the correlation studies which may improve the results obtained from the bivariational SCF level.

Later, the Auger and shape resonances of Be atom are studied. The dilated electron propagator is used up to the third order in conjunction with MSES. We have also characterized the effects of diffused functions in characterizing the shape resonances. The isoelectronic systems $^2\Pi_g$ N_2^-, $^2\Pi$ CO^- and $^2\Pi_g$ $C_2H_2^-$ are studied. The study is performed up to the bivariational SCF level only because these small molecular systems can be characterized at the bivariational SCF level itself. Different basis sets which are obtained by augmenting the standard basis set are used to study the effects. From this study, it is observed that in studying the $^2\Pi_g$ N_2^-, $^2\Pi$ CO^- and $^2\Pi_g$ $C_2H_2^-$ shape resonances, the additional diffused p-type orbitals have an important role, but the s- and d-type functions do not have major impacts.

Chapter 1

Introduction

In the usual formalism of quantum mechanics, the Hamiltonian operator H of the Schrödinger equation,

$$H\psi = E\psi, \tag{1.1}$$

is Hermitian, and consequently, the values of E are real and discrete. The corresponding wave functions ψ are square integrable and belong to the bound states of a system. However, the wave functions that are not square integrable correspond to continuum, scattering, or metastable states[1]. Thus, for a given quantum mechanical system, one can separate the spectrum into two types of solutions, one is bound states and another one is continuum states[2].

Resonances have been very popular for the last few decades in unveiling the mystery of atoms and molecules. Resonances are the results of electron-atom or electron-molecule scattering experiments[3, 4]. These are exponentially decaying long-lived metastable states of a system which can break into several subsystems as time elapses. Although the system has enough energy to break up, it takes a characteristic time to do so which is long enough to be characterized experimentally[5, 6].

The lifetime of these types of states can be found in the range of 10^{-13} to 10^{-15} s. Resonance states can be considered as discrete states that are embedded in the continuum. Therefore, treating these states becomes very challenging for quantum chemists as one has to deal with a continuum problem and electron correlation simultaneously[7].

1.1 Importance of Resonances

Resonances play an important role in diverse processes such as electron transport and energy exchange between electronic and nuclear motions. They are also involved in the vibrational excitation of molecules or molecular ions by electron impact, dissociative attachment, and recombination are important processes in outer space, in the higher atmosphere, and in plasma and discharges[8, 9].

In radio biology, large quantities of secondary low-energy electrons (LEEs) are generated due to the transfer of energy from ionizing radiation to molecules. These LEEs attach to DNA/RNA forming anionic metastable states (shape resonances) in DNA oligomers, DNA bases, and uracil. These metastable states dissociate into highly reactive anions and neutral radicals by dissociative electron attachment which may lead to DNA/RNA strands breaking, alteration to bases, sugar destruction, cross-link and dimer formation, and so forth. The study in this area has attracted researchers to a great extent in recent times [10–22]. The observations and findings from these studies will provide new advancements in the field of radiation therapy.

These transient species have been of great importance in various fields of the scientific world such as physics, chemistry, biology, and technology, e.g. attosecond[23, 24], X-ray spectroscopy[25], laser technology[26–28] etc. Resonances play an important role in the fabrication of quantum dots also[29, 30].

1.2 Mathematical Representations of the Resonances

In conventional quantum mechanics, the resonance states can be described by the evolution of wavepacket (propagating a wavepacket in time) obtained from the solution of the time-dependent Schrödinger equation (TDSE)

$$i\hbar\frac{\partial}{\partial t}\Psi(r,t) = \hat{H}\Psi(r,t). \tag{1.2}$$

The solutions of TDSE (1.2) for time-independent Hamiltonian are given by

$$\Psi(r,t) = \psi(r)e^{-iEt/\hbar} \tag{1.3}$$

where

$$E = E_R - i\frac{\Gamma}{2} \tag{1.4}$$

These complex energies are also known as Siegert energies. The real part (E_R) of the complex eigenvalue represents the position of resonance and the imaginary part ($\frac{\Gamma}{2}$) represents the half of the width of the resonance. The width of resonance (Γ) is inversely related to lifetime by the uncertainty relation $\Gamma = \frac{\hbar}{\tau}$. The imaginary part of E has a negative value to indicate the finite lifetime of metastable states[2].

This kind of study is usually challenging as one has to deal with a wavepacket rather than a single eigenstate. It is also obvious that the provision for complex energy leaves the possibility of having a finite lifetime. The use of TDSE leads to the following time-independent Schrödinger equation (TISE),

$$\hat{H}\psi(r) = E\psi(r) \tag{1.5}$$

which is similar to ordinary quantum mechanics which focuses on bound state problems, but the only difference is the energy value is complex as given in Eq. (1.4). In this case, the complex eigenvalues are obtained by imposing outgoing boundary conditions. Since in Hermitian quantum mechanics, complex energy is not possible, hence the Hamiltonian related to the above equation (1.5) must be non-Hermitian where the resonance energy is hidden in the continuum part. These complex resonance energies are associated with the complex poles of the scattering matrix (S-matrix).

To understand simply, let us consider a short-range one-dimensional potential V which tends to zero as $r \to \infty$. The eigenfunction of equation (1.5) at $r \to \infty$ can be written as a linear combination of the incoming e^{-ikr} and the outgoing e^{+ikr} plane waves with momenta $\mp k\hbar$

$$\psi(r \to \infty) = A(k)e^{-ikr} + B(k)e^{+ikr} \simeq e^{-ikr} + S(k)e^{+ikr} \tag{1.6}$$

with

$$E = \frac{(\hbar k)^2}{2\mu} \tag{1.7}$$

The S-matrix is defined as the ratio of amplitudes of outgoing waves to incoming waves, $S(k) = \frac{B(k)}{A(k)}$. There are two possibilities to obtain poles of S-matrix:

(1) When B(k) has poles. These are known as "false" poles which are not associated with the resonance phenomenon. These poles are independent of the potential.

(2) When the amplitude of the incoming waves, A(k), vanishes. These poles are associated with the bound states if these lie on the positive imaginary axis in the complex k-plane. On the other hand, the poles which are embedded in the fourth

quadrant of the complex k-plane ($\mathrm{Re}(k) > 0$ and $\mathrm{Im}(k) < 0$) are associated with the resonance phenomenon.

Therefore, the resonance wave functions obtained from equation (1.6) subject to the constraint that there is no incoming wave will have the following form

$$\psi(r \to \infty) = e^{ikr}, \quad S(k) \to \infty \tag{1.8}$$

which diverge asymptotically. Hence, the wave functions ψ are not in the Hilbert space, i.e., not square integrable which makes it difficult to solve the problem by standard electronic structure techniques. To deal with this problem modifications of standard electronic structure codes and specially designed approaches are required. Under such approaches, resonances are associated with complex eigenvalues[5, 6, 31].

1.3 Development of Analytical Continuation Methods

Different approaches have been developed by theoreticians that can be used to solve the problem by applying bound state-based methods to obtain resonances. These approaches include methods that explicitly solve the scattering problem as well as approaches that involve modifications of standard quantum chemistry packages. The list of latter includes stabilization method[3, 32], complex scaling[33–35], exterior complex scaling[36], complex basis function[37], complex absorbing potential[38–41], smooth exterior scaling[6, 42] and modified smooth exterior scaling[43].

Generally, the first approach used to adapt the purely bound state method was the stabilization method introduced by Hazi and Taylor[3, 32]. Using this technique one can reveal the resonance in the Hermitian domain. This technique is based on the scaling of basis functions where the resonance energy can be obtained from the stabilization plots of the energy eigenvalues as a function of an alternating stabilization parameter (α). However, it is challenging to obtain the real and imaginary components of resonance energy directly using this method from the stabilization graph. Therefore, it is followed analytical continuing the energy eigenvalue $E(\alpha)$ into the complex plane to obtain complex resonance energy from where real and imaginary components are extracted[17]. Although by applying the stabilization method one can get the best atomic results, since one has to repeat the eigenvalue computation for many values of stabilization parameter, it is not easy to extend the method for molecules. Also, by applying the stabilization method one cannot achieve the wave functions of resonance states[44]. A detailed discussion on the Hermitian Hamiltonian based quantum chemical methods for the calculation of resonances can be obtained in Chapter 3 of Ref.[6].

As the methods we are using in our work are based on the non-Hermitian Hamiltonian, special attention has been given on discussing such types of techniques. In non-Hermitian quantum mechanics, the wave function is not square integrable. Therefore, the basic idea of all these techniques is to convert the divergent wave function into a bounded normalizable function by carrying out a suitable mathematical transformation. By this way, wave functions become a part of Hilbert space[6]. A brief description of the underlying methods has been presented below.

1.3.1 Complex Scaling Method

One of the most widely used and successful methods is "complex scaling (CS) method " or "complex coordinate method" developed by Aguilar, Balslev, and Combes[33, 34] and Simon[35] in the early 1970s which provided a mathematical foundation for describing the resonance states. In this method, the dilation transformation of electronic coordinates $r \rightarrow \eta r$, where $\eta = e^{i\theta}$ is a complex number and θ is a real number called as scaling parameter, is used for the purpose. At the asymptote, the divergent wave function has the following form $\psi = e^{ikr}$. Under CS transformation, the wave function is changed into a dumping form as follows $\psi = e^{ikre^{i\theta}} = e^{ikrcos\theta}e^{-kxsin\theta}$ Then, the problem can be solved by bivariational self consistent field (SCF) using finite real basis functions providing discrete solutions of the following complex scaled Schrödinger equation:

$$H(\theta)\psi^{\theta} = E\psi^{\theta} \tag{1.9}$$

where $H(\theta) = U(\theta)HU^{-1}(\theta)$ with complex scaling operator $U(\theta) = e^{i\theta r\frac{\partial}{\partial r}}$.

The implementation of CS is very easy in studying atomic resonances. Therefore, CS method has been adapted with various bound state methods to calculate the resonance energies, e.g. SCF[45–47], Multiconfigurational SCF (MCSCF)[48, 49], Density Functional Theory (DFT)[50] etc.

However, the application of CS to study molecular resonances is not trivial. Although this method is very successful in the case of atomic systems, it becomes difficult in the case of molecular systems within the Born-Oppenheimer approximation. The CS requires the potential part of the Hamiltonian to be an analytical function[51]. If we apply CS to atoms, the Hamiltonian will take the following form

$$\hat{H}_{atom} = e^{-2i\theta}\hat{T}_e + e^{-i\theta}(\hat{V}_{eN} + \hat{V}_{ee}) \tag{1.10}$$

where $\hat{T}_e$ is the kinetic energy operator and $\hat{V}_{eN}$ and $\hat{V}_{ee}$ are electron-nucleus and electron-electron potential energy operators.

When CS is applied to molecules carrying out the following transformations

$$r_j \rightarrow e^{i\theta} r_j \tag{1.11}$$

$$R_k \rightarrow e^{i\theta} R_k \tag{1.12}$$

where $\{r_j\}$ and $\{R_k\}$ are the electronic and nuclear coordinates respectively and consequently the transformed Hamiltonian will have the following form

$$\hat{H}_{mol} = e^{-2i\theta}(\hat{T}_e + \hat{T}_N) + e^{-i\theta}(\hat{V}_{eN} + \hat{V}_{ee} + \hat{V}_{NN}) \tag{1.13}$$

where $\hat{T}_N$ is the kinetic energy operator of the nucleus and $\hat{V}_{NN}$ is the nucleus-nucleus potential energy operator. In the above equation (1.13), the coupling between electronic and nuclear coordinates through the electron-nuclei potential energy terms are not analytical operators. Therefore, it is not possible to use CS in molecular systems to obtain resonance parameters while keeping the nuclear positions fixed and unscaled[6]. However, Moiseyev and Corcoran[52] in 1979 showed that this difficulty can be overcome by carrying out analytical continuation of the Hamiltonian matrix elements instead of scaling the Hamiltonian[6]. This modified version of CS is used to study the shape resonances of molecular systems[53–59].

1.3.2 Exterior Complex Scaling Method

As the CS method encounters serious numerical difficulty while studying systems whose potential is not dilation analytic, Lipkin et al.[36] introduced the exterior

complex scaling (ECS) method based on Simon's[60] suggestion of keeping the coordinates on the real axis long enough to avoid any interior non-analiticities. In ECS method, the scaling is done in the external region only where the potential is dilation analytic. Here, the complex path in complex coordinate plane is defined as

$$z = \begin{cases} r, & r < r_0 \\ (r - r_0)e^{i\theta} + r_0, & r \geq r_0 \end{cases} \tag{1.14}$$

and the transformed Hamiltonian is given by

$$\hat{H}_\theta = -\frac{\hbar^2}{2M}\left[f^2(r)\frac{d^2}{dr^2} + (e^{-i\theta} - 1)\delta(r - r_0)\frac{d}{dr}\right] + V(z) \tag{1.15}$$

where the function f(r)is given by

$$f(r) \equiv \frac{dr}{dz} = \begin{cases} 1, & r < r_0 \\ e^{-i\theta}, & r \geq r_0 \end{cases} \tag{1.16}$$

Later, in the case of three-dimensional many-body problems, it becomes complicated to simplify the numerical calculations related to the resonance by using the ECS method. This problem arises because of the presence of a delta function potential term in the complex scaled Hamiltonian in equation (1.15)[6].

1.3.3 Complex Basis Functions Method

McCurdy and Rescigno[37] introduced the concept of the complex basis functions (CBFs) where no scaling of Hamiltonian is required. In this method, the transformation is applied to the basis set itself, where complex scaling is done to the exponential part of the basis function by a complex factor. As a result, to solve the resonance

problem, standard electronic structure code can be used provided Gaussian basis with complex exponents.

The CBFs method was applied to study the shape resonances in molecular systems[61–66]. However, it is needed to modify the existing electronic structure to a great extent while applying this method.

1.3.4 Complex Absorbing Potential

The motivation of applying complex absorbing potential (CAP) is very simple and obvious due to its simple implementation. Under the CAP method, the divergent resonance wave functions are converged into the physical domain of square integrable wave functions. When a wavepacket approaches the edge of a numerical grid artificial reflections occur and deteriorate the quality of the computed solution[43]. However, due to its nonphysical nature, it generates artificial perturbations of the system which may cause a shift in the energy [67]. The CAP is assumed to be zero in the interaction region and "turn on" where there are no interactions[68]. In practice, the CAP attenuates the asymptotic part of the wavepacket and hence suppresses the artificial reflections. The basic concept of CAP is to add an artificial complex potential to the unscaled Hamiltonian

$$H(\eta) = H - i\eta V_{CAP} \tag{1.17}$$

where V_{CAP} is one particle operator used to absorb the outgoing electron and η is CAP strength parameter.

In the CAP approach, the addition of complex potential makes the Hamiltonian non-Hermitian. However, the Hamiltonian matrix remains complex symmetric. The

additional complex potential causes an asymptotic damping of the Siegert wave function making the wave function square integrable and resulting discrete spectrum. However, one can obtain exact eigenfunction and eigenvalue only in the limit $\eta \to 0$ for a complete basis set. Practically, in realistic calculations incomplete basis sets are used and the CAP strength parameter η values have to get finite values. Therefore, it is only possible to minimize the perturbation by applying CAP, but can not make completely reflection free[69].

Different electronic structure methods augmented with CAP have been employed to study the atomic and molecular resonances[70–83]. Generally, the implementation of CAP in existing codes involves the perturbation of Hamiltonian by a CAP followed by the removal of artificial reflections generated by the CAP applying certain boundary conditions. The CAP was first introduced by Jolicard and co-workers[38, 39] for calculating the position and width of the resonance. Later, Riss and Meyer[40, 41] modified the basic concepts introduced by them and applied this to study the shape resonances. Manolopoulos[84] also derived transmission-free absorbing potential based on JWKB approximation which leads to less than 1% of reflection.

1.3.5 Smooth Exterior Scaling

A better alternative to CS and CAP methods is the smooth exterior scaling (SES), the so-called reflection-free CAP (RF-CAP) method [5, 68, 85–89]. SES is an efficient method based on the rigorous mathematical theory of CS to generate wave functions without any artificial reflections at the grid boundary and it doesn't disturb the interaction region. Hence, by applying SES similarity transformations to the Hamiltonian a reflection-free complex absorbing potential is generated. Basically, the SES shares the property of CAP[68] where the wavepacket is allowed to

propagate along an arbitrary smooth path in the complex coordinate plane, and the wavepacket gets absorbed when the path leaves the real axis[90]. In SES, the derivative of the scaling path ($[F(r)]$) is defined as

$$f(r) = \frac{\partial F}{\partial r} = 1 + [e^{i\theta_0} - 1]g(r) \tag{1.18}$$

such that $F(r) \to re^{i\theta_0}$ as $r \to \infty$.

where θ_0 is the scaling parameter and $g(r)$ goes smoothly from 0 to 1 around $r = r_0$, resulting in $f(r)$ going smoothly from 1 to $e^{i\theta_0}$. The SES Hamiltonian derived by Moiseyev is

$$\hat{H} = -\frac{\hbar^2}{2M}\frac{\partial^2}{\partial x^2} + V(F(r)) + V_{CAP} \tag{1.19}$$

where V_{CAP} is an energy-independent universal (non-local) complex absorbing potential (CAP). The SES Hamiltonian can be obtained by adding the universal CAP to the unscaled Hamiltonian. The SES has been used by Moiseyev and coworkers[51, 88] for electronic structure calculations to study the Feshbach-type autoionization resonances of atomic and molecular systems. A CAP which is similar to SES[91] is derived based on perfectly matched layer (PML) method that is extensively used to solve Maxwell's equations[92].

1.3.6 Modified Smooth Exterior Scaling

Kalita et al.[43] proposed and successfully applied the modified smooth exterior scaling (MSES) method in time-dependent dynamics problems. The MSES is a modified version of the SES method where the scaling function $\theta = \theta_0 a(r)$ is chosen as real which is complex in SES. In MSES, the scaling path ($[F(r)]$) is defined as

$$F(r) = re^{i\theta} = re^{i\theta(r)} = re^{i\theta_0 a(r)} \tag{1.20}$$

where $\theta(r)$ goes smoothly from 0 to θ_0 as $a(r)$ goes smoothly from 0 to 1. The scaling by the MSES method has been reported to be much smoother and displays efficient absorption during wavepacket propagation at the grid boundary[43, 93]. A detailed discussion of this method is presented in Chapter 2.

1.4 Goal and Motivation of this Thesis

The dilated Hamiltonian (complex scaled) produced by using any of the above mentioned bound state-based approaches becomes non-Hermitian and complex symmetric in nature. Since the complex scaled Hamiltonian loses the properties of the Hermitian operator, hence, the conventional SCF method becomes inapplicable to solve the problem. In this case, the resonant eigenvalues can be obtained by applying bivariational SCF method[46]. In this method, real basis functions are used with complex scaled Hamiltonian. This bivariational SCF method will be discussed in detail in Chapter 2.

The electron propagator theory[94] has been a powerful and effective tool in the direct calculation of electron detachment and electron attachment energies. The energy and width of resonances are related to the electron attachment energy (shape resonance) and electron removal energy (Auger resonance) of the metastable state. Therefore, the dilated electron propagator (complex scaled) method[47] has been applied successfully in characterizing the resonance parameters. This method is based on an underlying bivariational SCF method which preserves the formal structure of a real electron propagator and the resulting orbital energies are zeroth order poles and the corresponding amplitudes are Feynman-Dyson Amplitudes of dilated electron propagator[95]. Further, the orbital energies can be improved by using higher order perturbative decouplings of dilated electron propagator incorporating a greater

extent of relaxation and correlation effects. The theoretical background of dilated electron propagator theory has been discussed in detail in Chapter 2.

The main objective of this thesis is to formulate the analytical continuation method in bivariational SCF and electron propagator methods. MSES has been used as the analytical continuation tool along with SCF and electron propagator method. The motivation for these studies comes from the fact that

(1) MSES has been successfully applied to study the wavepacket propagation. It has also been proved that MSES can give better results than conventional SES methods.

(2) To the best of our knowledge, till now, MSES has not been used in electronic structure calculations.

(3) MSES shares and properties of CS but its application is very similar to that of CAP which is very easy to implement.

(4) The electron propagator theory is a straightforward method for improving the resonance energy and width obtained from bivariational SCF level.

The chapter-wise outline of the thesis is provided below.

This study involves the implementation of bivariational SCF-MSES method, dilated electron propagator method (dilated by MSES), and their application in studying electron-atom and electron-molecule scattering resonances. In the current chapter, we have already presented a brief description of metastable states. Different analytical continuation methods used in treating these states have also been discussed. The aim and scope of the present work have also been discussed in the last part of this chapter.

Chapter 2 discusses the basic concepts and the mathematical formulations of the methods used to study the electron scattering shape and Auger resonances in the present work. In this chapter, the MSES method to convert the divergent behavior of resonance wave functions to convergent or square integrable ones is discussed. Also, the bivariational SCF method used to solve the Schrödinger equation in non-Hermitian quantum mechanics and the dilated electron propagator method used to improve the resonance energy and width are summarized. The trajectory method to calculate the resonance energy is also included.

In **Chapter 3**, the shape resonances of isoelectronic systems $^2\Pi_g$ N_2^- and $^2\Pi$ CO^- are studied. Along with the MSES path, other three conventional SES paths are also tested. In this study, MSES is used for the first time in electronic structure calculation. The dilated electron propagator method is also used for up to second order to include the correlation studies which may improve the results obtained from bivariational SCF level. The results obtained are in good agreement with experimental results and other results from theoretical estimates. Unfortunately, except MSES path, we do not observe any stationary point for the other three conventional SES paths. This may be the reason that the conventional SES paths have not been applied to study the electron scattering shape resonances till now.

In **Chapter 4**, the Auger and shape resonances of Be atom are studied. The dilated electron propagator is used up to third order in conjunction with MSES. The resonance energy obtained for Auger resonance is in accordance with the experimental result. However, there are no experimental results available in the case of shape resonance to compare exactly. Therefore, the obtained results are compared with other theoretical estimates available in the literature. We use two different types of basis

sets to make our findings more reliable and the results from both the basis sets are close to each other and in good agreement with one of the latest theoretical estimates.

In **Chapter 5**, the effects of diffused functions in characterizing the molecular shape resonances are studied. The isoelectronic systems $^2\Pi_g$ N_2^-, $^2\Pi$ CO^- and $^2\Pi_g$ $C_2H_2^-$ are studied. The study is performed up to the bivariational SCF level only because these small molecular systems can be characterized at bivariational SCF level itself. Different basis sets which are obtained by augmenting the standard basis set are used to study the effects. The results obtained are compared to check the effects and discussed. From this study, it is observed that in studying the $^2\Pi_g$ N_2^-, $^2\Pi$ CO^- and $^2\Pi_g$ $C_2H_2^-$ shape resonances, the additional diffused p-type orbitals have an important role, but the s- and d-type functions do not have major impacts.

Chapter 6 gives an overview of the present work and the scope of the future works. In the first work, we applied the MSES in conjunction with the electron propagator to study the shape resonances in $^2\Pi_g$ N_2^- and $^2\Pi$ CO^- and obtained excellent results in comparison to experimental results. In addition, it is also observed that the other conventional SES paths fail to unveil the shape resonances. In the second work, we can obtain good results for Auger and shape resonances for Be. In the third work, we studied the effects of diffused basis functions and obtained that the additional p-type orbitals have a crucial role in characterizing the shape resonances in molecular systems.

Chapter 2

Methods Applied in Studying Shape and Auger Resonances

Resonances are quantized solutions of following TISE after applying outgoing boundary conditions

$$H\psi = E\psi. \tag{2.1}$$

which are associated with unstable quantum states (metastable states) with finite lifetime. These states are of quasi-bound character and lie hidden in the continuum part of the Hamiltonian. Therefore, the theoretical chemists are forced to apply bound state-based methods which have been discussed in Chapter 1 to uncover the resonances and to study the properties of these states. By applying these methods the resonance energies are obtained as complex eigenvalues $E = E_R - i\frac{\Gamma}{2}$ under the constraint that no incoming wave exists. One such method is MSES, which has been applied successfully to study resonance in dynamical systems[43].

In this Chapter, in the first section, we have formulated the necessary theoretical

framework for the MSES method in detail. In the subsequent sections, the bivariational SCF and the propagator theory are discussed. After that, the trajectory method to identify the resonance position and width has been discussed.

2.1 Modified Smooth Exterior Scaling Transformation

SES is a variant of the CS method. Here, the complex path is chosen in such a way that complex scaling is followed in the asymptotic limit. It is an efficient method to generate artificial reflection-free wave functions of dynamical systems. Basically, in this method, the wavepacket is allowed to propagate along an arbitrary (smooth) path in the complex coordinate plane and when the path leaves the real axis it gets absorbed. Users can keep as large a grid as their wish without being affected by the complex scaling. This is a very simple method to implement and most of the perturbation phenomenon of physical systems are avoided here. The effect of SES "turns on" only close to the end of the grid boundary. In SES, the scaling is done in the non-interaction region without affecting the interaction region, and hence, no scaling is required for the potential[68, 89]. The MSES is a modified form of SES. The fundamental difference between SES and MSES is that the scaling function θ is chosen as real in MSES which is complex in SES[43, 93].

Consider the following Schrödinger equation, with complex eigenvalue, $E = E_R - iE_I$,

$$\hat{H}\psi = E\psi \tag{2.2}$$

where

$$\hat{H} = -\frac{\hbar^2}{2M}\frac{\partial^2}{\partial z^2} + V(z) \tag{2.3}$$

Here, $z = F(x)$ is a path in the complex coordinate plane z, where

$$z = F(x) \to xe^{i\theta_0} \quad \text{as} \quad x \to \infty \tag{2.4}$$

On the basis of Simon's[60] proposition to avoid the scaling where the potential is non-dilation analytic, Rom et al.[67] defined the smooth-exterior scaling path as

$$f(x) = \frac{\partial F}{\partial x} = 1 + [e^{i\theta_0} - 1]g(x) \tag{2.5}$$

where $g(x)$ varies smoothly from 0 to 1 value around the point $x = x_0$. When $V(x \geq x_0) = 0$, then unscaled potential $V(x)$ can be used instead of complex potential $V(z)$.

It is easy to see from equations (2.4) and (2.5) that,

$$\frac{\partial}{\partial z} = f^{-1}(x)\frac{\partial}{\partial x} \tag{2.6}$$

then,

$$\begin{aligned}
\frac{\partial^2}{\partial z^2} &= \frac{\partial}{\partial z}(\frac{\partial}{\partial z}) = f^{-1}(x)\frac{\partial}{\partial x}(f^{-1}(x)\frac{\partial}{\partial x}) \\
&= f^{-1}(x)(-f^{-2}(x))\frac{\partial f(x)}{\partial x}\frac{\partial}{\partial x} + f^{-1}(x)f^{-1}(x)\frac{\partial^2}{\partial x^2} \\
\frac{\partial^2}{\partial z^2} &= -f^{-3}(x)\frac{\partial f(x)}{\partial x}\frac{\partial}{\partial x} + f^{-2}(x)\frac{\partial^2}{\partial x^2}
\end{aligned} \tag{2.7}$$

Therefore, the transformed Hamiltonian ($\hat{H}$) of equation (2.3) as derived by Moiseyev[96] can be written as:

$$\begin{aligned}
\hat{H} &= \frac{-\hbar^2}{2M}(-f^{-3}(x)\frac{\partial f(x)}{\partial x}\frac{\partial}{\partial x} + f^{-2}(x)\frac{\partial^2}{\partial x^2}) + V(z) \\
&= -\frac{\hbar^2}{2M}\frac{\partial^2}{\partial x^2} + \frac{\hbar^2}{2M}f^{-3}(x)\frac{\partial f(x)}{\partial x}\frac{\partial}{\partial x} + \frac{\hbar^2}{2M}\frac{\partial^2}{\partial x^2} - \frac{\hbar^2}{2M}f^{-2}(x)\frac{\partial^2}{\partial x^2} + V(z) \\
&= -\frac{\hbar^2}{2M}\frac{\partial^2}{\partial x^2} + \frac{1}{2}(\frac{\hbar^2}{M}f^{-3}(x)\frac{\partial f(x)}{\partial x})\frac{\partial}{\partial x} + (\frac{\hbar^2}{2M}(1 - f^{-2}(x)))\frac{\partial^2}{\partial x^2} + V(z) \\
\hat{H} &= -\frac{\hbar^2}{2M}\frac{\partial^2}{\partial x^2} + V[F(x)] + V_{CAP} \qquad (2.8)
\end{aligned}$$

where

$$\hat{V}_{CAP} = \frac{1}{2}V_1(x)\frac{\partial}{\partial x} + V_2(x)\frac{\partial^2}{\partial x^2} \qquad (2.9)$$

and

$$V_1(x) = \frac{\hbar^2}{Mf^3(x)}\frac{\partial f(x)}{\partial x} \qquad (2.10)$$

$$V_2(x) = \frac{\hbar^2}{2M}(1 - f^{-2}(x)) \qquad (2.11)$$

The volume element is given by

$$dz = f(x)dx \qquad (2.12)$$

The Hamiltonian can be transformed to simplify the expression of the volume element i.e., to make $dz = dx$. This can be carried out by defining a new function Φ,

$$\Psi(x) = f^{-\frac{1}{2}}\Phi(x) \qquad (2.13)$$

such that

$$\hat{H}_f = \frac{-\hbar^2}{2M}\nabla_f^2 + V[F(x)] \qquad (2.14)$$

where

$$\nabla_f^2 = f^{\frac{1}{2}}(x)\frac{\partial^2}{\partial z^2}f^{-\frac{1}{2}}(x) \tag{2.15}$$

After some algebraic calculations one can prove that $\Phi(x)$ is an eigenfunction of $\hat{H}^f$. Now, $\hat{H}_f$ can be redefined as

$$\hat{H}_f = -\frac{\hbar^2}{2M}\frac{\partial^2}{\partial x^2} + V[F(x)] + \hat{V}_{CAP}^f \tag{2.16}$$

$$\hat{H}_f = \hat{H} + \hat{V}_{CAP}^f \tag{2.17}$$

where,

$$\hat{V}_{CAP}^f = \hat{V}_{CAP}^{f(pot)} + \hat{V}_{CAP}^{f(kin)} \tag{2.18}$$

and $\hat{H} = -\frac{\hbar^2}{2M}\frac{\partial^2}{\partial x^2} + V[F(x)]$ is unscaled physical Hamiltonian. $\hat{V}_{CAP}^{f(pot)}$ and $\hat{V}_{CAP}^{f(kin)}$ are potential and kinetic terms of $\hat{V}_{CAP}^f$. Moiseyev and coworkers[51, 88] have discussed the conditions based on which the potential term $\hat{V}_{CAP}^{f(pot)}$ can be ignored. As discussed, the conditions are

(1) The repulsion between an electron in the outer (complex scaled) region and an electron in the inner (unscaled) region can be ignored as there is no double ionization of two correlated electrons.

(2) The scaling in SES is done only in the non-interaction region without affecting the interaction region and, hence, no scaling is required for the potential.

Hence, the $\hat{V}_{CAP}^f$ is reduced to

$$\hat{V}_{CAP}^f = \hat{V}_{CAP}^{f(kin)}, \tag{2.19}$$

which is an energy independent and universal reflection free CAP. The term $\hat{V}_{CAP}^{f(kin)}$ can be written as

$$\hat{V}_{CAP}^{f(kin)} = V_0(x) + V_1(x)\frac{\partial}{\partial x} + V_2(x)\frac{\partial^2}{\partial x^2} \tag{2.20}$$

The functions $V_1(x)$ and $V_2(x)$ are the same as defined in equations (2.10) and (2.11), where V_0 is defined as follow

$$V_0(x) = \frac{\hbar^2}{4M}f^{-3}(x)\frac{\partial^2 f}{\partial x^2} - \frac{5\hbar^2}{8M}f^{-4}(x)(\frac{\partial f}{\partial x})^2 \tag{2.21}$$

Now, in the usual implementation of SES, the $g(x)$[in equation (2.5)] can be defined with the help of a certain family of integration paths in complex coordinate plane e.g.,[68, 96]:

$$g(x) = 1 + 0.5(\tanh(\lambda(x - x_0)) - \tanh(\lambda(x + x_0))) \tag{2.22}$$

The path derived using this $g(x)$ is referred to as Path I[96]. The F(x) can be derived by carrying out the integration over $g(x)$. Thus, the $F(x)$ will have the following form for the path given in the equation (2.22):

$$F(x) = x + (e^{i\theta} - 1)[x + \frac{1}{2\lambda}\ln\frac{\cosh[\lambda(x - x_0)]}{\cosh[\lambda(x + x_0)]}] \tag{2.23}$$

Along with Path I, there exist several other paths that are based on polynomials $g(x) \sim x^p$ or Gaussians. Some well-known paths are

Path II[68, 89]

$$g(x) = (1 + e^{(x_0 - x)\lambda})^{-1} + (1 + e^{(x_0 + x)\lambda})^{-1}, \tag{2.24}$$

$$F(x) = x + (e^{i\theta} - 1)[2x - \frac{1}{\lambda}ln(1 + e^{(x_0 + x)\lambda}) + \frac{1}{\lambda}ln(1 + e^{(x_0 - x)\lambda}) \tag{2.25}$$

Path III[86, 89]

$$g(x) = \begin{cases} 0, & x \leq x_0 \\ 1 - e^{-\lambda(x-x_0)^2} + 2\lambda(x-x_0)^2 e^{-\lambda(x-x_0)^2}, & x > x_0 \end{cases} \tag{2.26}$$

$$F(x) = \begin{cases} x, & x \leq x_0 \\ x + (e^{i\theta} - 1)(x - x_0)(1 - e^{-\lambda(x-x_0)^2}), & x > x_0 \end{cases} \tag{2.27}$$

SES following implementation using these paths will be termed as conventional SES (CSES). In this method, $g(x)$ is taken as real. Scaling function $\theta(x)$ and path $F(x)$ are related by the following relation

$$F(x) = xe^{i\theta(x)} \tag{2.28}$$

resulting in $\theta(x)$ becoming complex.

At the asymptote, when the potential vanishes, the resonance wave function will have the form as follows

$$\psi = e^{ikx}.$$

After applying complex scaling $x \to xe^{i\theta}$, ψ will be converted as

$$\psi = e^{ikxe^{i\theta}} = e^{ikx\cos\theta} e^{-kx\sin\theta}.$$

In the above equation, the second term of ψ is responsible in making the wave function square integrable. But, as in case of CSES, if we consider θ as complex i.e., $\theta = \theta_r + i\theta_{im}$, the wave function will take the following form

$$\psi = e^{ikxe^{i\theta_r}e^{-\theta_{im}}} = e^{ikx\cos\theta_r e^{-\theta_{im}}} e^{-kx\sin\theta_r e^{-\theta_{im}}}$$

and it is evident that θ_{im} does not serve any purpose.

Therefore, in MSES, the scaling function $\theta(x)$ is chosen as real, which makes the $g(x)$ complex. The real function $\theta(x)$ is defined as

$$\theta(x) = \theta = a(x)\theta_0 \tag{2.29}$$

where θ_0 is scaling parameter and $a(x)$ is chosen as:

$$a(x) = 1 + 0.5(\tanh(\lambda(x - x_0)) - \tanh(\lambda(x + x_0))) \tag{2.30}$$

The value of $a(x)$ varies from 0 to 1 around the point $x = x_0$.

Now, to calculate the $g(x)$ for MSES, after taking first derivative of equation (2.28), we get

$$\frac{\partial F}{\partial x} = f(x) = e^{i\theta} + ixe^{i\theta}\frac{\partial \theta}{\partial x} \tag{2.31}$$

By comparing equations (2.5) and (2.31), we have

$$g(x) = \frac{e^{i\theta} - 1}{e^{i\theta_0} - 1} + ix\frac{e^{i\theta}}{e^{i\theta_0} - 1}\theta_0\frac{\partial a(x)}{\partial x} \tag{2.32}$$

Differentiating $a(x)$ of equation (2.30) with respect to x and putting the value of $\frac{\partial a(x)}{\partial x}$ in equation (2.32), we get the form of g(x) as follow

$$g(x) = \frac{e^{i\theta} - 1}{e^{i\theta_0} - 1} + ix\frac{e^{i\theta}}{e^{i\theta_0} - 1}\theta_0\lambda 0.5[\text{sech}^2(\lambda(x - x_0)) - \text{sech}^2(\lambda(x + x_0))] \tag{2.33}$$

The SES using this $g(x)$ is referred to as MSES method and the corresponding path will be defined as

$$z = F(x) = xe^{i\theta(x)} = xe^{ia(x)\theta_0}. \tag{2.34}$$

To compare the efficiency of CSES and MSES paths, the complex paths $F(x)$ have been plotted for both methods in Fig.2.1. For CSES, the Path I is used. The scaling parameters used for both the complex paths are $\theta_0 = 0.32$, $\lambda = 0.28$ a.u., and $x_0 = 360$ a.u. A detailed comparison of both methods can be seen in Ref.[43].

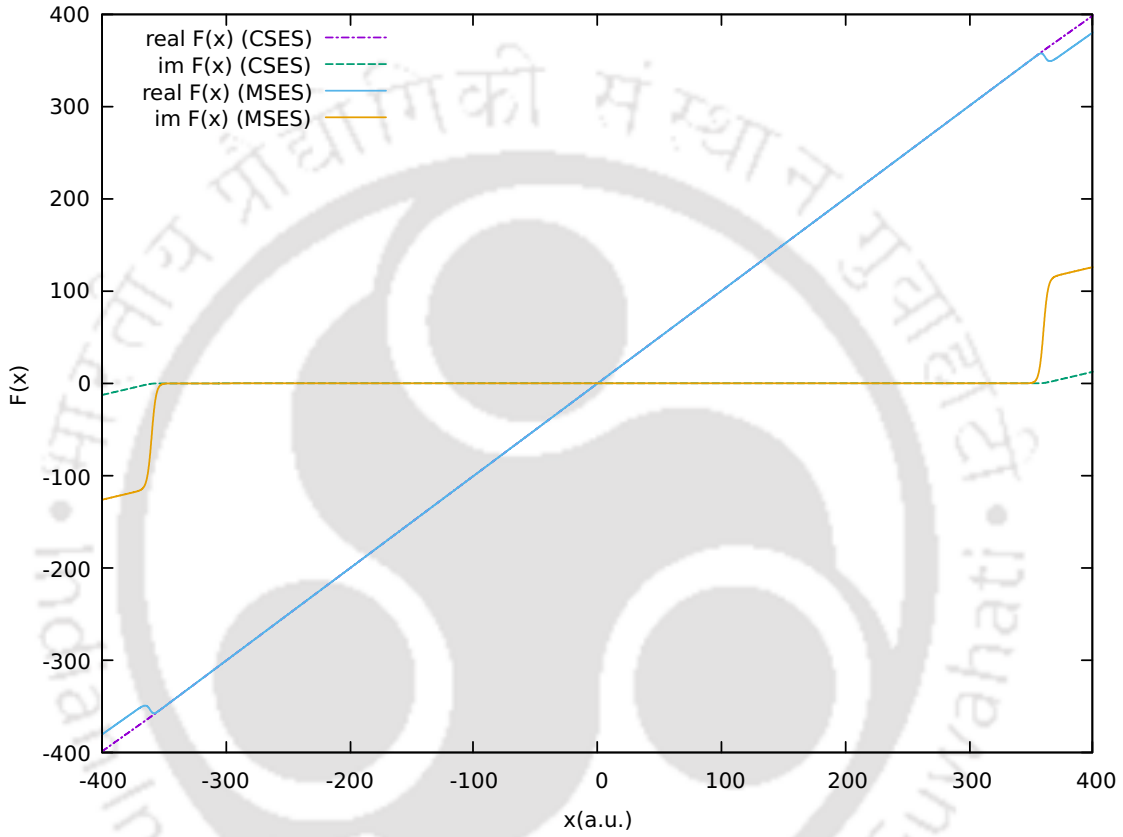

FIGURE 2.1: Plot of $F(x)$ vs x for CSES and MSES methods

The difference between CSES and MSES is not only in the path but in the formulation also. In MSES, the function $\theta(x)$ is chosen as real which is complex in the case of CSES. As a result, the function $g(x)$ becomes complex in MSES which is real in the case of CSES. In Ref.[43], the MSES method has been applied to time-dependent and time-independent problems. In the case of a time-dependent problem, the MSES is used as an absorbing potential similar to the application of negative imaginary potential/CAP. It is observed that the MSES method is better by at least 7 orders of magnitude as compared to the CSES during the absorption of the wavepacket. In

CSES, as the scaled region (where the CAP is generated) is decreased keeping other parameters fixed, the results deteriorate by 5 orders of magnitude while the results from the MSES remain mostly unchanged. It shows the robustness of the MSES and implies that the MSES method can provide better reflection-free CAP .

In the same publication, for a time-independent problem, CS, CSES, and MSES methods have been applied to calculate resonances during the photodissociation of H_2^+ molecule. It is observed that the results obtained from the CSES method differ significantly from the benchmark result obtained by using CS with a very high number of grid points converged to at least 8 digits. However, results obtained from CS and MSES methods are indistinguishable. So, it has been concluded that the MSES method is far better than the CSES method in calculating resonance states.

In our formulation, $F(x)$ is dependent on three parameters, x_0, θ_0, and λ. The value of x_0 is chosen such that only within the interval $-x_0 < x < x_0$ of x the physical potential $V(x)$ can have non-zero values and vanishes elsewhere. The parameter λ is associated with an effective size of the intermediate region where $F(x) \neq x$ and $F(x) \neq xe^{i\theta_0}$. For larger values of λ, this intermediate region becomes smaller and the SES path is obtained. For $\lambda = 0$, the usual CS path, $z = xe^{i\theta_0}$, is obtained. At the limit of $\lambda \to \infty$ the SES transformation is reduced to ECS transformation and

$$z = \begin{cases} x, & -x_0 \leq x \leq x_0 \\ (x - x_0)e^{i\theta_0} + x_0, & x > x_0 \\ (x + x_0)e^{i\theta_0} - x_0, & x < -x_0 \end{cases} \tag{2.35}$$

The MSES has been successfully applied to absorb the wavepacket in the grid boundary and obtained promising results in comparison to CSES[43]. Now, we are using this method on the more general case of three-dimensional many-particle systems.

To implement it to the standard *ab initio* electronic structure package, a practical approach is to carry out the transformation in the Cartesian coordinates,

$$F(r) = (F(x), F(y), F(z)) \tag{2.36}$$

where

$$F(r) = re^{i\theta} \tag{2.37}$$

and r stands for x or y or z. In our calculations $x_0 = y_0 = z_0$.

2.2 Bivariational SCF

The complex scaled Hamiltonian (dilated by MSES) $H(\eta)$ has the following form

$$H_f(\eta) = \sum_i \left(-\frac{\hbar^2}{2M}\nabla_i^2 - \frac{Z}{r_i} \right) + \sum_{i<j} \frac{1}{r_{ij}} + \hat{V}_{CAP}^f \tag{2.38}$$

where $\eta = e^{i\theta}$. $H_f(\eta)$ loses the properties of the Hermitian operator and becomes non-Hermitian preserving the complex symmetric property, i.e., $H_f^\dagger(\eta) = H_f^\star(\eta) \neq H_f(\eta)$ due to the complex value of η. As a result, the conventional variational theorem becomes inapplicable. Therefore, the bivariational SCF method[46] is applied to solve the problem related to complex symmetric operators. The only difference between the conventional SCF (or the usual Hartree Fock theory) and bivariational SCF is that in the latter the solution provides complex eigenvalues.

In the complex SCF method (also known as bivariational SCF)[46, 47], the dilated Hamiltonian is used along with real basis functions. To apply the bivariational SCF

method, the functional

$$E(\Phi_0, \Psi_0) = \frac{< \Phi_0 | H(\eta) | \Psi_0 >}{< \Phi_0 | \Psi_0 >} \tag{2.39}$$

is extremized to obtain the bivariational SCF equations with conditions Φ_0 and Ψ_0 should be single determinants

$$\Phi_0 = (N!)^{-\frac{1}{2}} \det\{\phi_i(x_i)\} \tag{2.40}$$

$$\Psi_0 = (N!)^{-\frac{1}{2}} \det\{\psi_j(x_j)\} \tag{2.41}$$

where $i = j = 1, 2, ..., N$ and the constituent one-electron orbitals ϕ and ψ be biorthonormal

$$< \phi_i | \psi_j >= \delta_{ij} \tag{2.42}$$

Following SCF equations can be obtained by extremizing the functional equation (2.39)

$$\Omega \phi_i = \epsilon_i \phi_i \tag{2.43}$$

$$\Omega^{+} \psi_i = \epsilon_i^{\star} \psi_i \tag{2.44}$$

where

$$\Omega_1(\eta, \phi, \psi) = -\frac{\hbar^2}{2M} \nabla_1^2 - \sum_A \frac{Z_A}{r_{1A}} + \int_{x_{2'}=x_2} \frac{(1 - P_{12})}{r_{12}} \rho(x_{2'}, x_2) dx_2 + \hat{V}_{CAP}^f(r_1) \tag{2.45}$$

with

$$\rho = \sum_i^{occ} \phi_i \psi_i^{\star} \tag{2.46}$$

and

$$\hat{V}_{CAP}^f(r) = \hat{V}_{CAP}(x) + \hat{V}_{CAP}(y) + \hat{V}_{CAP}(z) \tag{2.47}$$

The $\hat{V}_{CAP}(x)$ is defined in equation (2.18).

The dilated Hamiltonian is complex symmetric, i.e., $H^{\dagger}(\eta) = H^{\star}(\eta)$. Since the choice of basis function has the property as Φ=$\Psi^{\star}$, the many-electron wave function satisfies the same relation. The detailed implementation and the advantages of bivariational SCF is described in Ref. [46].

Diagonalization of complex symmetric matrices can lead to self-orthogonality of the eigenstates. To check the correctness of the result diagonalization of the complex symmetric Fock matrix is carried out by two different methods (i) the *LAPACK* subroutine for general complex matrix diagonalization (ZGEEV) and (ii) the method developed by Bar-On et al.[97] for complex symmetric matrices. Both methods provide indistinguishable results. Our group has studied resonance coalescence for the parameters where coalescence or exceptional points occur and found that both methods break down to diagonalize the complex symmetric matrices[98]. While applying these methods in computing complex eigenvalues, we do not encounter any problems in obtaining eigenvalue solutions.

To evaluate

$$\langle p(x,y,z)|\hat{V}_{CAP}(x)|q(x,y,z)\rangle \tag{2.48}$$

where $p(x,y,z)$ and $q(x,y,z)$ are primitive Gaussian basis, defined as

$$p(x,y,z) = N_p x^l y^m z^n e^{-\alpha(r-r_0)^2} \tag{2.49}$$

and centered at r_0=(x_0, y_0, z_0).

$p(x,y,z)$ can be written as

$$p(x,y,z) = N_p p_x p_y p_z \tag{2.50}$$

where $p_x = x^l e^{-\alpha(x-x_0)^2}$ and similarly p_y and p_z. Hence, the expression (2.48) can be partitioned as

$$N_p N_q \langle p_x p_y p_z | \hat{V}_{CAP}(x) | q_x q_y q_z \rangle = N_p N_q \langle p_x | \hat{V}_{CAP}(x) | q_x \rangle \langle p_y | q_y \rangle \langle p_z | q_z \rangle \tag{2.51}$$

where $\langle p_y | q_y \rangle$ and $\langle p_z | q_z \rangle$ are evaluated analytically and $\langle p_x | \hat{V}_{CAP}(x) | q_x \rangle$ being a one dimensional integral is evaluated numerically.

2.3 The Electron Propagator

The electron propagator theory[94] is a powerful tool for improving the electron affinities (EA) and ionization potentials(IP) that are calculated from the bivariational SCF level. As the resonance energies are associated with the EA and IP, it is obvious that the dilated electron propagator[47] can be used for the direct calculation of resonance energies and widths of electron-atom and electron-molecule scatterings. The higher-order dilated electron propagator provides a systematic framework for improving the results obtained from the bivariational SCF[46] level by incorporating the relaxation and correlation effects. These improvements can be made by introducing an effective potential, called self-energy, which was formulated by Dyson[99]. This method has been proven as an effective and convenient method in characterizing Auger and shape resonances in atomic[100–102] and molecular systems[53, 54, 58].

The Dyson equation for dilated electron propagator $\mathbf{G}$ can be written as[54]

$$\mathbf{G}(\eta, E) = \mathbf{G}_0(\eta, E) + \mathbf{G}_0(\eta, E)\Sigma(\eta, E)\mathbf{G}(\eta, E) \tag{2.52}$$

where $\mathbf{G}_0(\eta, E)$ is known as the zeroth order dilated electron propagator and is a matrix of the electron propagator of uncorrelated electron motion and $\Sigma(\eta, E)$ is defined as

$$\Sigma(\eta, E) = \Sigma^{(2)}(\eta, E) + \Sigma^{(3)}(\eta, E) + ... \tag{2.53}$$

$\Sigma(\eta, E)$ is the matrix representation of the exact self-energy on the basis of spin orbitals which is the sum of different orders such as second order, $\Sigma^{(2)}(\eta, E)$, and third order, $\Sigma^{(3)}(\eta, E)$. This self-energy matrix contains the relaxation and correlation effects.

In particular, the elements of the second order self-energy matrix are given as follows[94, 99]

$$\Sigma^{(2)}_{ij}(\eta, E) = \frac{1}{2}\sum_{ars} \frac{< rs||ia >< ja||rs >}{E(\eta) + \epsilon_a(\eta) - \epsilon_r(\eta) - \epsilon_s(\eta)} + \frac{1}{2}\sum_{abr} \frac{< ab||ir >< jr||ab >}{E(\eta) + \epsilon_r(\eta) - \epsilon_a(\eta) - \epsilon_b(\eta)} \tag{2.54}$$

where the indices a,b,... represent occupied spin orbitals, r,s,... represent unoccupied spin orbitals and i,j,... represent unspecified orbitals, and the antisymmetric two-electron integral is given by

$$< ij||kl >= \eta^{-1} \int \psi_i(1)\psi_j(2)\frac{(1 - P_{12})}{r_{12}}\psi_k(1)\psi_l(2)dx_1dx_2. \tag{2.55}$$

The third order energy dependent (ED) part of the dilated self energy matrix is given by[102]

$\Sigma^{(3)}_{ED}(\eta, E) =$

$$\frac{1}{4}\sum_a\sum_b\sum_p\sum_q\sum_r \frac{< ip||qr >< qr||ab >< ab||jp >}{(E(\eta)+\epsilon_p(\eta)-\epsilon_a(\eta)-\epsilon_b(\eta))(\epsilon_a(\eta)+\epsilon_b(\eta)-\epsilon_q(\eta)-\epsilon_r(\eta))} \tag{2.56}$$

$$-\sum_a\sum_b\sum_c\sum_p\sum_q \frac{< ic||qb >< qp||ac >< ab||jp >}{(E(\eta)+\epsilon_p(\eta)-\epsilon_a(\eta)-\epsilon_b(\eta))(\epsilon_a(\eta)+\epsilon_c(\eta)-\epsilon_p(\eta)-\epsilon_q(\eta))} \tag{2.57}$$

$$+\frac{1}{4}\sum_a\sum_b\sum_p\sum_q\sum_r \frac{< ip||ab >< ab||qr >< qr||jp >}{(E(\eta)+\epsilon_p(\eta)-\epsilon_a(\eta)-\epsilon_b(\eta))(\epsilon_a(\eta)+\epsilon_b(\eta)-\epsilon_q(\eta)-\epsilon_r(\eta))} \tag{2.58}$$

$$-\sum_a\sum_b\sum_c\sum_p\sum_q \frac{< iq||ac >< ab||pq >< pc||jb >}{(E(\eta)+\epsilon_q(\eta)-\epsilon_a(\eta)-\epsilon_c(\eta))(\epsilon_a(\eta)+\epsilon_b(\eta)-\epsilon_p(\eta)-\epsilon_q(\eta))} \tag{2.59}$$

$$-\frac{1}{4}\sum_a\sum_b\sum_c\sum_d\sum_p \frac{< ip||ab >< ab||cd >< cd||jp >}{(E(\eta)+\epsilon_p(\eta)-\epsilon_c(\eta)-\epsilon_d(\eta))(E(\eta)+\epsilon_p(\eta)-\epsilon_a(\eta)-\epsilon_b(\eta))} \tag{2.60}$$

$$+\sum_a\sum_b\sum_c\sum_p\sum_q \frac{< iq||cb >< cp||aq >< ab||jp >}{(E(\eta)+\epsilon_p(\eta)-\epsilon_a(\eta)-\epsilon_b(\eta))(E(\eta)+\epsilon_q(\eta)-\epsilon_b(\eta)-\epsilon_c(\eta))} \tag{2.61}$$

$$+\frac{1}{4}\sum_a\sum_b\sum_c\sum_p\sum_q \frac{< ic||ab >< ab||pq >< pq||jc >}{(E(\eta)+\epsilon_c(\eta)-\epsilon_p(\eta)-\epsilon_q(\eta))(\epsilon_a(\eta)+\epsilon_b(\eta)-\epsilon_p(\eta)-\epsilon_q(\eta))} \tag{2.62}$$

$$-\sum_a\sum_b\sum_p\sum_q\sum_r \frac{< ir||aq >< ab||pr >< pq||jb >}{(E(\eta)+\epsilon_b(\eta)-\epsilon_p(\eta)-\epsilon_q(\eta))(\epsilon_a(\eta)+\epsilon_b(\eta)-\epsilon_q(\eta)-\epsilon_r(\eta))} \tag{2.63}$$

$$+\frac{1}{4}\sum_a\sum_b\sum_c\sum_p\sum_q \frac{< ia||pq >< pq||bc >< bc||ja >}{(E(\eta)+\epsilon_a(\eta)-\epsilon_p(\eta)-\epsilon_q(\eta))(\epsilon_b(\eta)+\epsilon_c(\eta)-\epsilon_p(\eta)-\epsilon_q(\eta))} \tag{2.64}$$

$$-\sum_a\sum_b\sum_p\sum_q\sum_r \frac{< ib||pr >< pq||ab >< ar||jq >}{(E(\eta)+\epsilon_b(\eta)-\epsilon_p(\eta)-\epsilon_r(\eta))(\epsilon_a(\eta)+\epsilon_b(\eta)-\epsilon_p(\eta)-\epsilon_q(\eta))} \tag{2.65}$$

$$+\frac{1}{4}\sum_a\sum_p\sum_q\sum_r\sum_s \frac{< ia||pq >< pq||rs >< rs||ja >}{(E(\eta)+\epsilon_a(\eta)-\epsilon_r(\eta)-\epsilon_s(\eta))(E(\eta)+\epsilon_a(\eta)-\epsilon_p(\eta)-\epsilon_q(\eta))} \tag{2.66}$$

$$-\sum_a\sum_b\sum_p\sum_q\sum_r \frac{< ib||rq >< ra||pb >< pq||ja >}{(E(\eta)+\epsilon_a(\eta)-\epsilon_p(\eta)-\epsilon_q(\eta))(E(\eta)+\epsilon_b(\eta)-\epsilon_q(\eta)-\epsilon_r(\eta))} \tag{2.67}$$

The third order energy independent dilated self energy matrix is also given as follow

$$\Sigma_{EI}^{(3)}(\eta) =$$

$$\frac{1}{2}\sum_a\sum_b\sum_p\sum_q\sum_r \frac{< ir||jp >< ab||rq >< pq||ab >}{(\epsilon_a(\eta)+\epsilon_b(\eta)-\epsilon_p(\eta)-\epsilon_q(\eta))(\epsilon_a(\eta)+\epsilon_b(\eta)-\epsilon_q(\eta)-\epsilon_r(\eta))} \tag{2.68}$$

$$-\frac{1}{2}\sum_a\sum_b\sum_c\sum_p\sum_q \frac{< ia||jc >< cb||pq >< pq||ab >}{(\epsilon_a(\eta)+\epsilon_b(\eta)-\epsilon_p(\eta)-\epsilon_q(\eta))(\epsilon_b(\eta)+\epsilon_c(\eta)-\epsilon_p(\eta)-\epsilon_q(\eta))} \tag{2.69}$$

$$+\frac{1}{2}\sum_a\sum_b\sum_p\sum_q\sum_r \frac{< ip||ja >< ab||qr >< qr||pb >}{(\epsilon_a(\eta)+\epsilon_b(\eta)-\epsilon_q(\eta)-\epsilon_r(\eta))(\epsilon_a(\eta)-\epsilon_p(\eta))} \tag{2.70}$$

$$-\frac{1}{2}\sum_a\sum_b\sum_c\sum_p\sum_q \frac{< ip||ja >< bc||pq >< aq||bc >}{(\epsilon_b(\eta)+\epsilon_c(\eta)-\epsilon_p(\eta)-\epsilon_q(\eta))(\epsilon_a(\eta)-\epsilon_p(\eta))} \tag{2.71}$$

$$+\frac{1}{2}\sum_a\sum_b\sum_p\sum_q\sum_r \frac{< ia||jr >< rb||pq >< pq||ab >}{(\epsilon_a(\eta)+\epsilon_b(\eta)-\epsilon_p(\eta)-\epsilon_q(\eta))(\epsilon_a(\eta)-\epsilon_r(\eta))} \tag{2.72}$$

$$-\frac{1}{2}\sum_a\sum_b\sum_c\sum_p\sum_q \frac{< ic||jp >< pq||ab >< ab||cq >}{(\epsilon_a(\eta)+\epsilon_b(\eta)-\epsilon_p(\eta)-\epsilon_q(\eta))(\epsilon_c(\eta)-\epsilon_p(\eta))} \tag{2.73}$$

Now, multiplying equation (2.52) by $(\mathbf{G}_0(\eta,E))^{-1}$ and $(\mathbf{G}(\eta,E))^{-1}$ on left and right side respectively, we get

$$(\mathbf{G}_0(\eta,E))^{-1} = (\mathbf{G}(\eta,E))^{-1} + \Sigma(\eta,E) \tag{2.74}$$

In terms of a set of occupied and unoccupied spin orbitals generated from the solution of bivariational SCF equations, the matrix elements of $\mathbf{G}_0^{-1}(\eta,E)$ are

$$[\mathbf{G}_0^{-1}(\eta,E)]_{ij} = (E-\epsilon_i)\delta_{ij} \tag{2.75}$$

where ϵ is the diagonal matrix of eigenvalues i.e., is the orbital energy of the ith spin orbital and is the zeroth order pole of the dilated electron propagator.

Now by using Eq. (2.75), the propagator in Eq. (2.74) can be written

$$(\mathbf{G}(\eta, E))^{-1} = (\mathbf{G}_0(\eta, E))^{-1} - \Sigma(\eta, E) = E1 - \epsilon(\eta) - \Sigma(\eta, E) \tag{2.76}$$

Since the inverse of a matrix does not exist when its determinant is zero, the roots of the following energy dependent equation correspond to the poles of the dilated electron propagator

$$\det(E1 - \epsilon(\eta) - \Sigma(\eta, E)) = 0 \tag{2.77}$$

When $\Sigma(\eta, E)$=0, the poles occur at ϵ_i can be called as Zeroth order dilated electron propagator (ZoDEP) which is the same as that of the bivariational SCF level[103]. Since ϵ is diagonal, to calculate the lowest order correction, we are ignoring the off-diagonal elements of self energy ($\Sigma(\eta, E)$)[94, 99]. Consequently, the associated pole search becomes easy, just by solving the following equation

$$E(\eta) = \epsilon(\eta) + \Sigma_{ii}(\eta, E) \tag{2.78}$$

where E is an electron binding energy. The solution can be done repeatedly starting with $E = \epsilon_i$ until the convergence result is found. The lowest-order correction with second order self energy to ϵ_i is given by the following equation

$$\epsilon_i' = \epsilon_i + \Sigma_{ii}^{(2)}(\epsilon_i) \tag{2.79}$$

From now onwards, the zeroth order dilated electron propagator based on MSES will be referred to as ZoDEP-MSES and will also be called as Bivariational SCF-MSES

method. Similarly, the second order and third order dilated electron propagators will be referred to as SoDEP-MSES and ToDEP-MSES respectively.

2.4 Calculation of Resonance Energy Using Trajectory Method

As mentioned in section 2.1, the MSES method depends on three parameters, x_0, λ, and θ_0. A resonance is observed as a stationary point which is obtained by plotting θ_0-trajectories keeping all other parameters fixed. In this type of θ_0-trajectory, a resonance is associated with a single cusp where the absolute value of the velocity of the trajectory gets a minimum value. Although the MSES depends on several parameters, a resonance is associated with a single stationary point on a θ_0-trajectory[51]. Thus, at optimum, the resonance eigenvalue follows

$$\left(\frac{\partial E}{\partial \theta_0}\right)_{\lambda_{optimum}, x_{0optimum}} = 0 \tag{2.80}$$

The Eq. 2.80 can be solved by plotting θ_0-trajectory where the resonance energy (E) is plotted as a function of θ_0 keeping all other parameters fixed. This method of solution is known as the graphical method. The stabilization point along the θ_0-trajectories [plots of Re(E) vs Im(E)] satisfying complex virial theorem leads to cusp, kinks, loops, or any kind of "slow down"[104].

Chapter 3

Application of Modified Smooth Exterior Scaling Method to Study $^2\Pi_g$ N_2^- and $^2\Pi$ CO^- Shape Resonances

In this chapter, the MSES method is applied for the first time to calculate the energy and the width of the electron-molecule scattering. The isoelectronic $^2\Pi_g$ N_2^- and $^2\Pi$ CO^- shape resonances have been studied as a test case for the MSES method. The results obtained using this method are in good agreement with experimental results. The CSES method with different paths has also been applied for comparison purposes.

3.1 Introduction

Resonances are one of the most important phenomena in electron-molecule scattering. The first and most famous example, as well as application, was forwarded by Gamow[105] when he studied the α-decay of heavy nuclei in 1928.

The resonance energies in atomic and molecular systems are related to IP and EA, which are calculated as the difference between the ground state total energies of the $(N \pm 1)$ and the neutral target that can be calculated using Koopman's theorem[99]. In general, $IP = (E_s(N-1) - E_0(N)) = -\epsilon_s$ and $EA = (E_0(N) - E_s(N+1)) = -\epsilon_s$, where s labels a stationary state and $E_0(N)$ is the ground state total energy of the neutral N electron target, and the resonance energy and width are calculated as negative of IP and EA i.e., ϵ_s which are known as Auger and shape resonances respectively. The corresponding resonance wave functions are not L^2-integrable. By carrying out a dilation transformation of the electronic coordinates, the resonance wave functions become square integrable. Mathematically, this transformation is the analytical continuation of Hamiltonian in the complex plane. Different techniques that can be used for this purpose have already been discussed in Chapter 1

Bivariational SCF[46, 47], a complex scaled version of conventional SCF, had been implemented to study the resonance states in atomic [100, 101, 103, 106] and molecular systems [107, 108]. In this work, an attempt has been made to study the resonance states under the MSES. Hence, the method we are using here to study will be referred to as bivariational SCF-MSES. The results obtained from bivariational SCF should improve by incorporating relaxation and correlation effects. So, to include these effects, the second order dilated (complex scaled by MSES) electron propagator (SoDEP-MSES) method is applied. This is the first time to use MSES method to study the shape resonances of molecular systems.

The necessary theoretical background of MSES, bivariational SCF, and the electron propagator has been discussed in Chapter 2. In the next section, results are shown and discussed along with two subsections, the $^2\Pi_g$ N_2^- shape resonance and the $^2\Pi$ CO^- shape resonance. Finally, conclusions are made with some future prospects and endeavor of the underlying method.

3.2 Results and Discussion

The isoelectronic systems $^2\Pi_g$ N_2^- and $^2\Pi$ CO^- have been the prototypical systems used to test the effectiveness of new theoretical methods in treating molecular shape resonances. We apply the bivariational SCF-MSES and SoDEP-MSES methods to study the molecular shape resonances. We are testing the efficacy of the MSES method using the mentioned systems. Atomic units are used throughout unless otherwise stated. The basis set we employed to study $^2\Pi_g$ N_2^- and $^2\Pi$ CO^- shape resonances is aug-cc-pCVDZ with augmentation. The basis set for all the atoms is augmented for the accommodation of an electron of the metastable state. The most diffused functions of type s and p are augmented by multiplying the factor of $\frac{1}{2^n}$ for $n = 1, 2, \cdots, 5$. Hence, the augmented basis functions will be referred to as aug-cc-pCVDZ+5s5p(A).

Although the MSES method generally depends on several parameters as mentioned in Chapter 2, a resonance is associated with a stabilization point (cusp) in a plot when the resonance energy is plotted as a function of θ_0 keeping other parameters fixed. We have performed a series of calculations for various x_0 and λ parameters, and the value of parameter λ is chosen as 10.0 a.u. from the set of well stabilized resonance θ_0-trajectories. The same value of λ is also applied by Y. Sajeev et al. to study the Feshbach type autoionization resonance of Helium[88] and hydrogen

molecule[51]. The corresponding θ_0-trajectories have been plotted using the respective x_0 values for $^2\Pi_g$ N_2^- and $^2\Pi$ CO^- shape resonances.

3.2.1 The $^2\Pi_g$ N_2^- shape resonance

The $^2\Pi_g$ N_2^- shape resonance is perhaps the most studied molecular resonance among electron-molecule scattering problems studied so far. The basis set aug-cc-pCVDZ+5s5p(A) is employed for each nitrogen atom. The N_2 molecule is placed along the x-axis symmetrical to the origin considering the bond length of 1.09 Å. For bivariational SCF-MSES method, the θ_0-trajectories using different complex scaling paths i.e., MSES Path, Path-I, Path-II, and Path-III, are plotted in Figure 3.1. Same values of different parameters are used for all the paths (λ=10.0 and x_0=4.5). We have not added any dc field[51, 88] to the Hamiltonian either in CSES or in MSES. In the figure, no clear stationary points (i.e., cups or kinks) are observed except for MSES path.

In Figure 3.1, in the case of MSES path, there are many closely spaced curves which contain kinks or stationary points. Out of many kinks shown in the figure, only one of them represents $^2\Pi_g$ N_2^- shape resonance, which is shown by an arrow. Others are artifacts due to an incomplete basis set. Whether a state is resonance or artifact can be identified by plotting the orbital wave function[109]. A resonance state is localized within the interaction region, but a continuum or artifacts will be localized outside the interaction region. As the SES does not affect the interaction region, the shape of molecular orbitals in the interaction region does not get distorted much. Therefore, we have plotted the molecular orbitals at the stationary point to check which curve belongs to the $\pi_g^\star$ state. The orbital corresponding to that state is plotted in Figure 3.2, which shows a typical $\pi_g^\star$ character of the lowest unoccupied molecular orbital

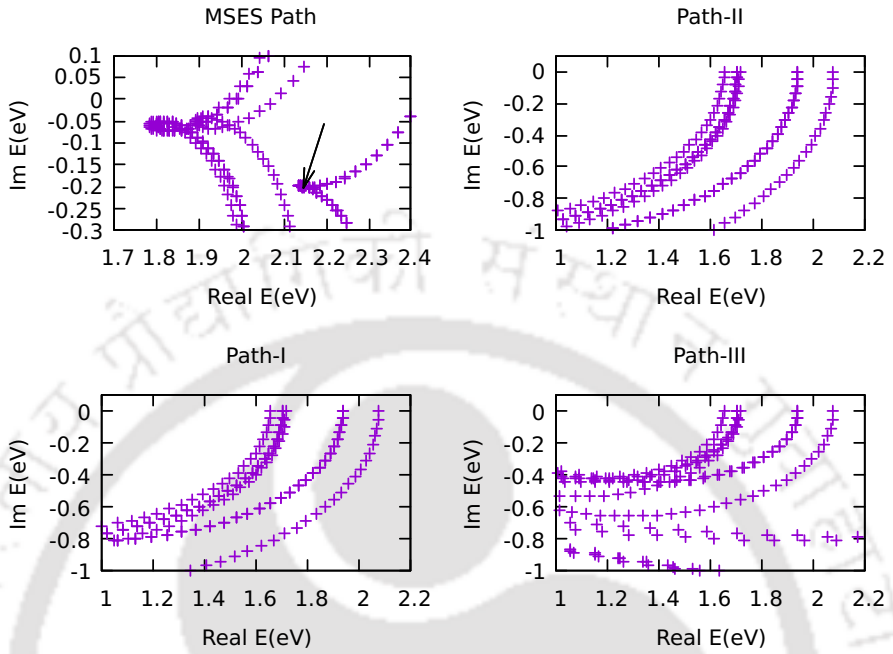

FIGURE 3.1: θ_0-trajectories of orbital energies of N_2 for x_0=4.5 using MSES Path, Path-I, Path-II and Path-III. Cups are seen only for MSES path. The arrow shows the position of $^2\Pi_g$ N_2^- shape resonance. Other cups are artifacts as concluded after plotting orbitals.

(LUMO). Only the real part of the orbital is plotted, as the imaginary part is an order smaller than the real part. If the absolute value of the wave function is plotted, then the nodal structure will be lost. The corresponding resonant-θ_0-trajectory is displayed in Figure 3.3. The optimal θ_0 value at the stationary point is 0.24. The values of energy and width obtained from the real and imaginary part of the resonant pole are 2.14 eV and 0.39 eV respectively. The SoDEP-MSES method is employed to improve the results obtained from the bivariational SCF level. The resonant-θ_0-trajectory for SoDEP-MSES is given in Figure 3.4. The results obtained from both bivariational SCF-MSES and SoDEP-MSES methods show no discernible difference. S. Mahalakshmi et al.[58] also reported no considerable change while performing

a higher-order dilated electron propagator to the $^2\Pi_g$ N_2^- shape resonance. The same conclusion can be drawn from this work. McCurdy et al.[109] also indicated that some well-known molecular shape resonances (N_2^-, CO^-, F_2^-, etc.) can be characterized at the bivariational SCF level itself. The energy and width obtained from the bivariational SCF-MSES and SoDEP-MSES methods along with other theoretical methods and experiment results are collected in Table 3.1. As compared to other theoretically calculated results, the results obtained from bivariational SCF-MSES and SoDEP-MSES methods are in good agreement with experimental results.

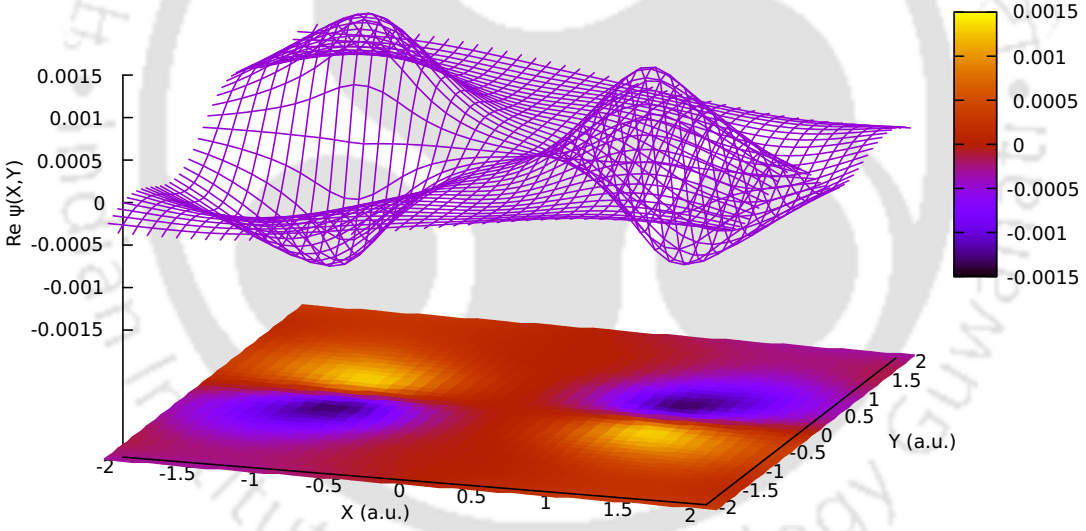

FIGURE 3.2: The resonance wave function of $^2\Pi_g$ N_2^- shape resonance. The positions of two N atoms are at 0.545 and -0.545 along x-axis.

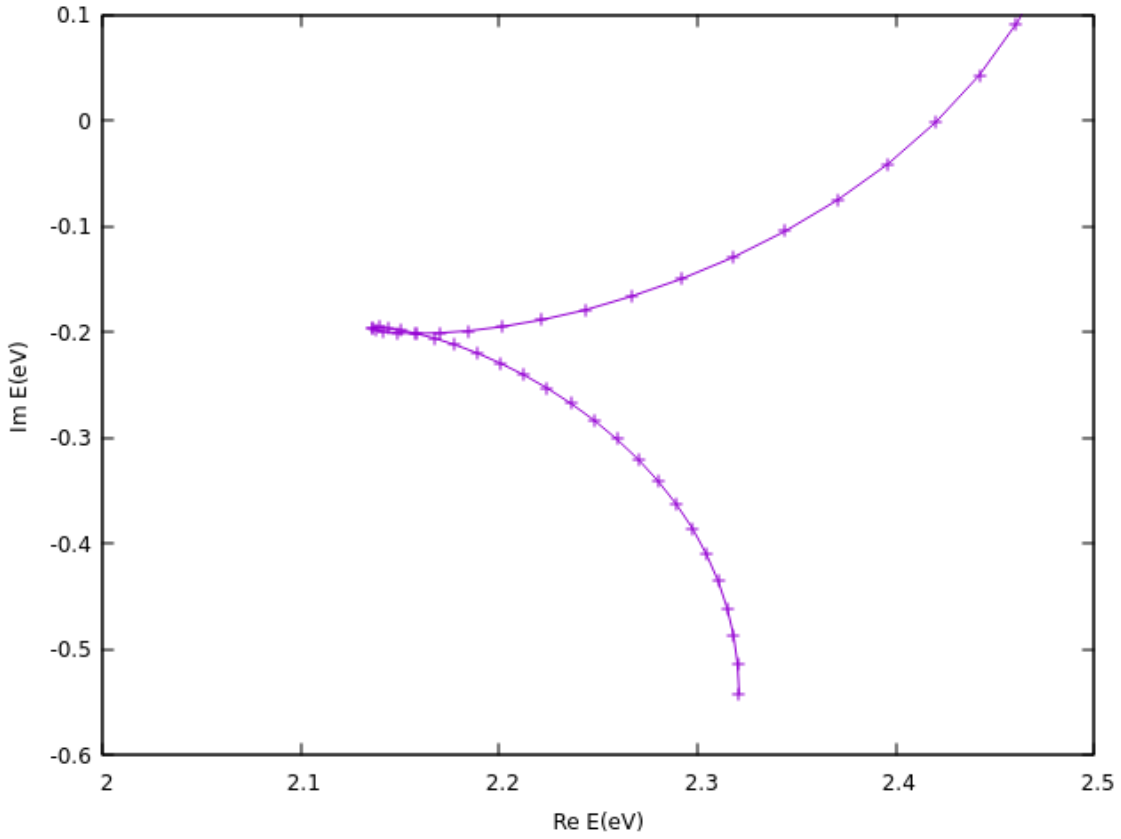

FIGURE 3.3: θ_0-trajectory of $^2\Pi_g$ N_2^- shape resonance at x_0=4.5 using bivariational SCF-MSES.

3.2.2 The $^2\Pi$ CO^- shape resonance

The basis set employed to investigate $^2\Pi$ CO^- shape resonance is aug-cc-pCVDZ+5s5p(A) centered on C and another aug-cc-pCVDZ+5s5p(A) centered on O. The CO molecule is set along the x-axis symmetrical to the origin considering the bond length 1.128 Å. For the bivariational SCF-MSES method, using the same values of different parameters (λ=10.0, x_0=3.3), θ_0-trajectories for four different paths (i.e., MSES path, Path-I, Path-II, and Path-III) are plotted as displayed in Figure (3.5) without adding any dc field to the Hamiltonian.

In Figure 3.5, no clear stationary points are observed except for the MSES path. So, in the MSES path, to confirm which curve belongs to the $^2\Pi$ state, we have plotted

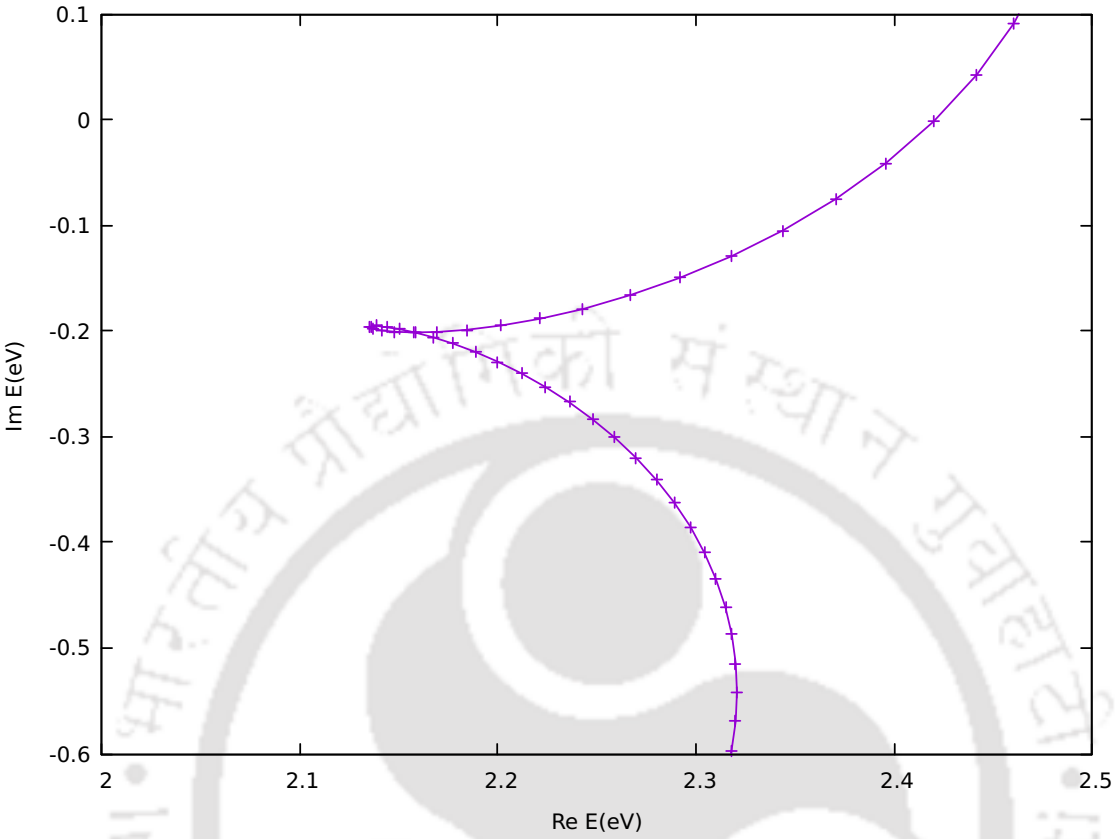

FIGURE 3.4: θ_0-trajectory of $^2\Pi_g$ N_2^- shape resonance at x_0=4.5 using SoDEP-MSES.

the molecular orbitals at the stationary points. The orbital corresponding to that state is plotted in Figure 3.6, which is a $\pi^\star$ LUMO with greater amplitude on the carbon atom[58]. As in the case of the $^2\Pi_g$ N_2^- shape resonance, we have plotted only the real parts of the orbital. The corresponding resonant-θ_0-trajectory has been plotted in Figure 3.7. The value of the resonance energy and width obtained from this work along with other theoretical methods and experimental results are displayed in Table 3.2. We would like to mention that the energy and width that are obtained in our calculation are 1.57 eV and 0.49 eV respectively. The reported optimal value of θ is 0.34 at the stationary point. As in the case of the $^2\Pi_g$ N_2^- shape resonance, here also SoDEP-MSES is applied. The resonant-θ_0-trajectory for the SoDEP-MSES method is displayed in Figure 3.8. The resonance position

Method	Energy (eV)	Width (eV)
Experiment[110]	2.32	0.41
Linear algebric method[111]	2.13	0.31
Static exchange R-matrix[112]	2.15	0.34
Stabilization method[113]	2.44	0.32
Boomerang model[114]	1.91	0.54
Complex SCF[115]	3.19	0.44
Second order dilated electron propagator(real SCF)[116]	2.14	0.26
CAP-FSMRCC[72]	2.52	0.39
dp-CAP-EOM-EA-CCSD($r_j^{CAP} \neq 0$)[74]	2.57	0.26
rm-CAP-EOM-EA-CCSD($r_j^{CAP} \neq 0$)[76]	2.50	0.35
rm-CAP-EOM-EA-CCSD($r_j^{CAP} = 0$)[76]	2.53	0.32
EOM-EA-CCSD[66]	2.54	0.52
MCSCF-CAP[79]	3.12	0.31
CAP/EA-ADC(3)[117]	2.54	0.40
CAP/PP-CASSCF[83]	3.83	0.25
Results from biorthogonal dilated electron propagator[58]		
Zeroth order, quasi particle second order and quasi particle diagonal 2ph-TDA	2.12	0.19
Second order	2.11	0.18
Diagonal 2ph-TDA	2.12	0.18
Quasi-particle/OVGF third order	2.11	0.18
Third order	2.11	0.18
Bivariational SCF-MSES (This work)	2.14	0.39
SoDEP-MSES (This work)	2.14	0.39

TABLE 3.1: Energy and Width of $^2\Pi_g$ N_2^- shape resonance

.

obtained from the SoDEP-MSES method shows improvement. However, the results obtained from both bivariational SCF-MSES and SoDEP-MSES methods are very close to the experimental results and in good agreement with the other results that are obtained from various theoretical methods.

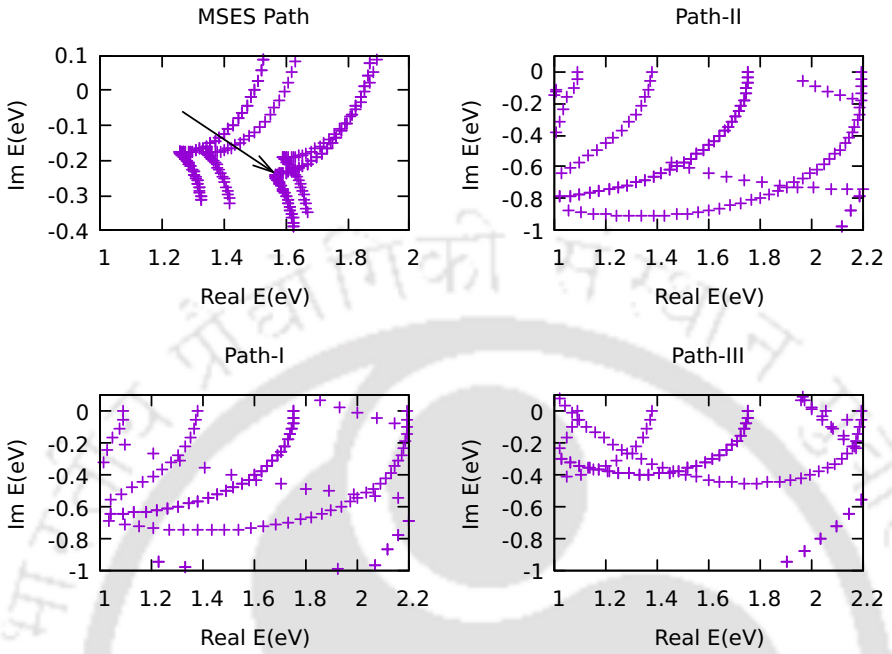

FIGURE 3.5: θ_0-trajectories of orbital energies of CO for x_0=3.3 using MSES Path, Path-I, Path-II and Path-III. Cups are seen only for MSES path. The arrow shows the position of $^2\Pi$ CO^- shape resonance. Other cups are artifacts as concluded after plotting orbitals.

3.3 Conclusion

In this chapter, bivariational SCF-MSES and SoDEP-MSES methods have been applied for the first time to study the shape resonances in electron-molecule scattering. The $^2\Pi_g$ N_2^- and $^2\Pi$ CO^- shape resonances have been studied. The results obtained in this work using the MSES method compare well with experimental results. Also, we perform a comparison with different complex scaling paths. It is clear that conventional SES can not be used as-is to study the shape resonance. From this work, it is also observed that bivariational SCF-MSES and SoDEP-MSES methods give

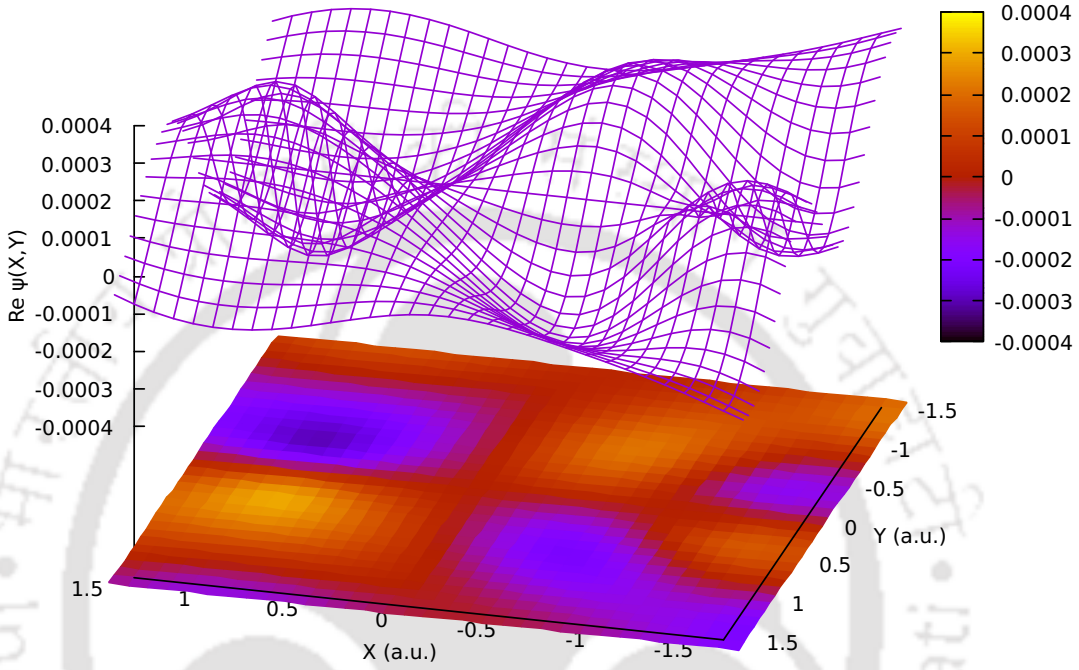

FIGURE 3.6: The resonance wave function of $^2\Pi$ CO^- shape resonance. The positions of C and O atoms are at 0.564 and -0.564 along x-axis respectively.

better results than calculations done using other methods. Therefore, we can conclude that the MSES method is quite reliable and effective in investigating molecular shape resonances.

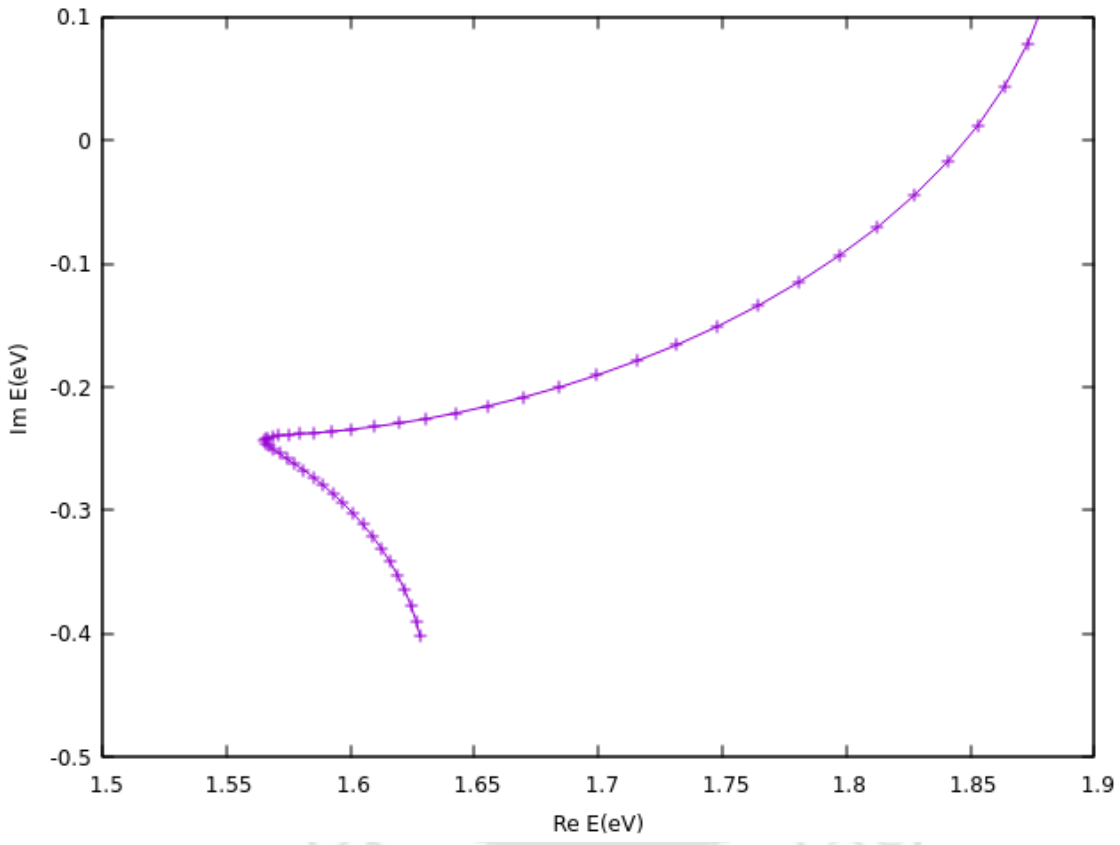

FIGURE 3.7: θ_0-trajectory of $^2\Pi$ CO^- shape resonance at x_0=3.3 using bivariational SCF-MSES.

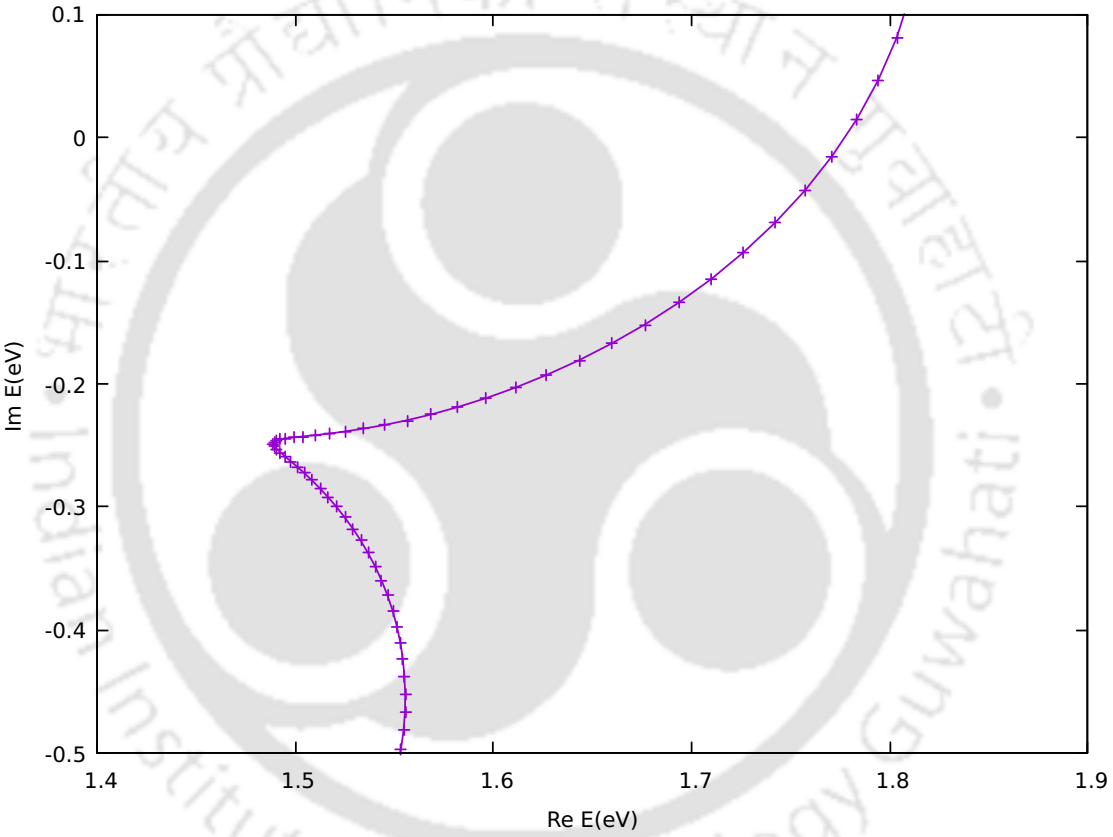

FIGURE 3.8: θ_0-trajectory of $^2\Pi$ CO^- shape resonance at x_0=3.3 using SoDEP-MSES.

Method	Energy (eV)	Width (eV)
Experiment[118]	1.50	0.40
Boomerang model[119]	1.52	0.80
Close coupling method[120]	1.75	0.28
Second order dilated electron propagator(real SCF)[121]	1.71	0.10
dp-CAP-EOM-EA-CCSD($r_j^{CAP} \neq 0$)[74]	1.98	0.59
rm-CAP-EOM-EA-CCSD($r_j^{CAP} \neq 0$)[76]	2.01	0.60
rm-CAP-EOM-EA-CCSD($r_j^{CAP} = 0$)[76]	2.09	0.61
EOM-EA-CCSD[66]	2.04	1.03
MCSCF-CAP[79]	1.28	0.32
CAP/EA-ADC(3)[117]	1.95	0.63
CAP/PP-CASSCF[83]	2.16	0.31
Results from bi-orthogonal dilated electron propagator[58]		
Zeroth order, quasiparticle second order and quasiparticle diagonal 2ph-TDA	1.71	0.10
Second order	1.68	0.09
Diagonal 2ph-TDA	1.69	0.08
Quasi-particle third order and OVGF third order	1.65	0.14
Third order	1.65	0.14
Bivariational SCF-MSES (This work)	1.57	0.49
SoDEP-MSES (This work)	1.49	0.50

TABLE 3.2: Energy and Width of $^2\Pi$ CO^- shape resonance.

Chapter 4

Use of Dilated Electron Propagator in Conjunction with Modified Smooth Exterior Scaling Method to Characterize Auger and Shape Resonances in Be

In this chapter, the dilated electron propagator method in conjunction with MSES has been utilized to characterize the Auger and shape resonances in Be. The MSES method is an efficient method to impose outgoing boundary conditions in electron-atom or electron-molecule scatterings. MSES can be used to convert divergent wave functions to square integrable ones. The dilated electron propagator has been proven to be an efficient and powerful tool in characterizing the Auger and shape resonances. Resonance energies obtained by using this method are in good agreement with experimental results and other theoretical estimates available in the literature.

4.1 Introduction

In e-atom and e-molecule scattering following process may be observed ($\star$ represents the metastable state)

$$e + A \rightarrow (A^-)^\star \rightarrow A + e. \tag{4.1}$$

In the above process, an incoming particle (i.e., an electron) with a specific kinetic energy collides with target A, combines with it to produce a quasi-bound anionic state or a resonance state $(A^-)^\star$, and decays by emitting an electron. The resonances which are energetically above the parent state are called "shape resonances" or "negative ion resonances"[4]. The resonance energy (i.e., the kinetic energy) of the incoming particle for which resonance is observed, is obtained from the reaction (4.1) as follows

$$E_{res} = E_{(A^-)^\star} - E_A = E_s^{N+1} - E_0^N \tag{4.2}$$

which is equal to the EA of the target A. Here, s represents the resonance state of the target anion and E_0^N denotes the total ground state energy of the N-electron target.

Similarly, the Auger resonances are considered as an emission of a core electron from the target following the formation of an auto-ionizing hole. During the Auger process, a core electron of the target is removed by an external mechanism (i.e., by photon or electron). The Auger resonances may be, schematically, represented as follows

$$h\nu + A \rightarrow (A^+)^\star + e \tag{4.3}$$

$$(A^+)^\star \rightarrow A^{++} + e \tag{4.4}$$

and the corresponding resonance energy is given by the following equation

$$E_{res} = E_A - E_{(A^+)^\star} = E_0^N - E_s^{N-1} \tag{4.5}$$

which is equal to the IP of the target A for obtaining $(A^+)^\star$[1, 103]. From these relations, a crude approximation of resonance energies can be obtained through Koopmans' theorem[99] by calculating complex orbital energies. Thus, this approach can provide both energy and width of electron detachment Auger resonance and electron attachment shape resonances.

The complex resonance energies can be obtained by imposing purely outgoing boundary conditions on the wave functions of the time-independent non-Hermitian Hamiltonian. The associated wave functions are not square integrable and diverge asymptotically. Further, the correlation and relaxation effects also have an important role in characterizing the metastable states. Hence, the solution to these types of problems requires the simultaneous treatment of both continuum and correlation treatment. In dealing with such problems, the computational difficulties are more than those encountered in the case of bound states. So, the method of analytical continuation of Hamiltonian has to be performed in the complex plane to make the resonance function square integrable[5, 6].

In Chapter 3, we have applied the MSES method to study the shape resonances in molecular systems and excellent results of resonance energy and width have been reported. In that work, we used the SoDEP in conjunction with MSES (SoDEP-MSES). In this work, an attempt has been made to study the ^{2}S Be$^+$ ($1s^{-1}$) Auger resonance and ^2P Be$^-$ shape resonance by applying dilated electron propagator (dilated by MSES) up to third order. Literature admits a lot of studies in the investigation of $1s^{-1}$ Auger hole in Be and results so obtained are in level of acceptable

agreement with the experimental result. Our results of Be obtained by applying third-order dilated electron propagator underlying MSES (ToDEP-MSES) match very closely with the experimental result and are much better than other theoretical results published so far. Unfortunately, the ^2P Be^- shape resonance has not been studied experimentally so far. Therefore, the results from this calculation are compared with other theoretically calculated results available in the literature.

The necessary theoretical background of MSES, bivariational SCF and the electron propagator has been discussed in Chapter 2. In section 4.2, we are discussing about the computational details, and results and present the data and required figures obtained from our work. Finally, in section 4.3, a summary of our findings is presented.

4.2 Results and Discussion

Generally in CS or MSES, we search for a stabilization point in a graph where the resonance energy is plotted as a function of scaling parameters. It has already been mentioned in Chapter 2 that in the case of MSES, a resonance is associated with a single stationary point on a θ_0-trajectory plotted keeping other parameters fixed. The optimal values of parameters x_0 and λ are chosen as 4.5 a.u. and 10.0 a.u. respectively from a set of well stabilized resonance trajectories. The same value of λ has also been used for investigating other systems[51, 88]. We have also used the same value of λ in Chapter 3.

4.2.1 ^2S Be^+ $(1s^{-1})$ Auger resonance

The ^2S Be^+ $(1s^{-1})$ Auger resonance has served as a prototypical scheme in testing the effectiveness of new theoretical techniques in the study of Auger resonances.

Therefore, to check the utility of dilated electron propagator in conjunction with MSES in characterizing Auger resonances in atomic systems, the $1s^{-1}$ Auger hole in Be is investigated as a test case. The qualitative and quantitative details of the ^2S Be^+ ($1s^{-1}$) Auger resonance have been studied extensively. In the case of Auger resonances, since resonant eigenvalues have a negative imaginary part to represent the finite lifetime of the metastable state and the target ground state is completely real, the poles will have the positive imaginary part. Therefore, the resonant-θ_0-trajectories will move to the first quadrant of the complex energy plane and the poles displayed in the first quadrant may represent the Auger resonances[53, 122].

The basis set used to study $1s^{-1}$ Auger hole in Be is $14s11p$ which has been used earlier by various researchers[102, 106, 123]. Using this basis set, the θ_0-trajectories from ZoDEP-MSES, SoDEP-MSES and ToDEP-MSES are plotted in figures (4.1), (4.2) and (4.3) respectively. For all the plots, stabilization points are observed at θ_0=0.14 radians. The results obtained from different order of dilated electron propagators are collected in Table 4.1 along with other theoretically calculated and experimental results.

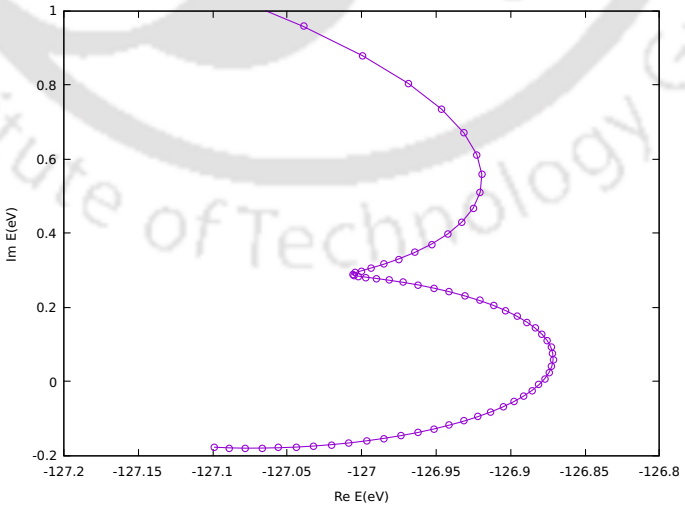

FIGURE 4.1: θ_0-trajectory of ^2S Be^+ ($1s^{-1}$) Auger resonance at x_0=4.5 using bivariational SCF-MSES (ZoDEP-MSES).

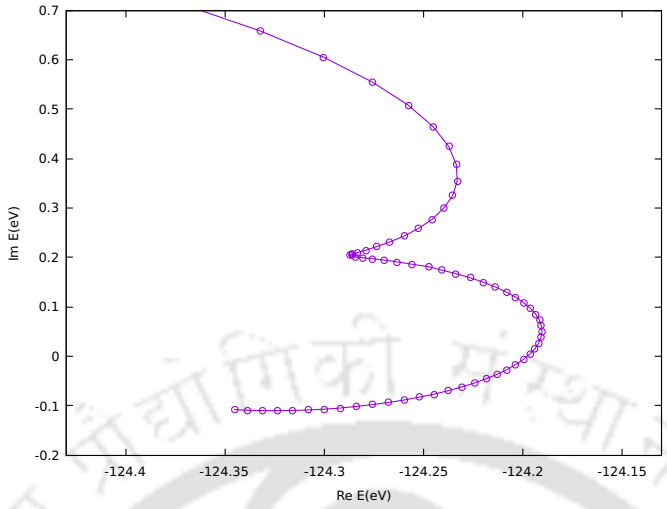

FIGURE 4.2: θ_0-trajectory of ^2S Be^+ $(1s^{-1})$ Auger resonance at x_0=4.5 using SoDEP-MSES.

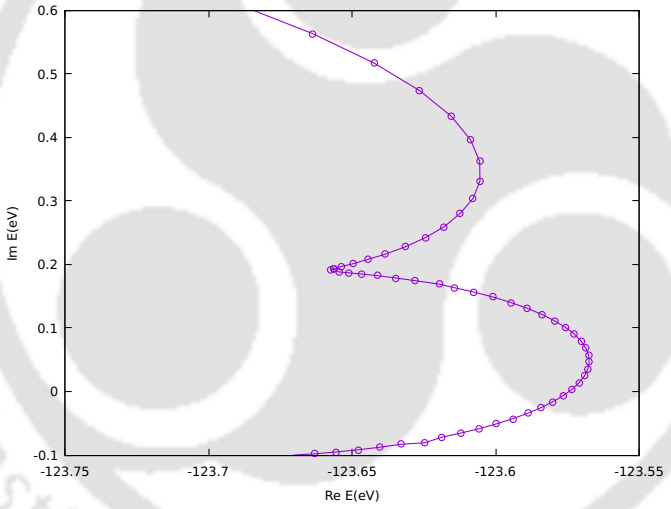

FIGURE 4.3: θ_0-trajectory of ^2S Be^+ $(1s^{-1})$ Auger resonance at x_0=4.5 using ToDEP-MSES.

The resonance energy obtained from ZoDEP-MSES is very far from the experimental result. This is due to the non-inclusion of relaxation and correlation effects. However, a clear distinction between the continuum and resonance state has been observed. After applying SoDEP-MSES, the resonance energy is obtained as 124.29 eV and the width is 0.41 eV. This lowering in energy is due to the inclusion of correlation and relaxation effects which lead to some additional screening of the nucleus

Method	Energy (eV)	Width (eV)
Experiment[124, 125]	123.63	-
Many-body perturbation theory[126]	-	0.09
Second order electron propagator with Siegert boundary condition[127]	125.47	0.02
Fock space MRCC (14s11p basis)[106]	123.82	0.45
Results from bi-orthogonal dilated electron propagator(14s11p)		
Zeroth order[123]	128.80	0.24
quasiparticle diagonal 2ph-TDA[123]	127.90	0.54
Diagonal 2ph-TDA[123]	125.43	0.02
quasiparticle second order[123]	124.98	0.05
Second order[102]	125.34	0.22
Third order[102]	124.63	0.76
ZoDEP-MSES (This work)	127.01	0.58
SoDEP-MSES (This work)	124.29	0.41
ToDEP-MSES (This work)	123.66	0.38

TABLE 4.1: Energy and Width of ^2S Be^+ ($1s^{-1}$) Auger resonance.

by the electron. Further, the width also decreased because of the increased relaxation time. Subsequently, the energy obtained after applying ToDEP-MSES is closer to the experimental results. However, there is no experimental result available to compare the width. However, the width obtained from this calculation is comparable with the most recent estimate from Fock space MRCC[106] with the same basis set. From this picture, it is clear that the Auger decay is a correlated event and its characterization at the bivariational SCF level (ZoDEP) is meaningless. However, we include the result from the bivariational SCF level to highlight the requirement of correlation and relaxation effects in the study of Auger resonances. The results obtained from this calculation are in good agreement with experimental results.

4.2.2 ^2P Be^- shape resonance

The low-lying ^2P Be^- shape resonance has been extensively studied theoretically by various researchers[49, 75, 79, 83, 102, 109, 128–134]. This resonance also serves as the prototypical system for testing the new techniques in electron scattering shape resonances in the case of atomic systems. To study this resonance problem, Venkatnathan et al.[135] found that uncontracted $14s11p$ basis set as the best in their case. Originally, this basis set was derived from $10s$ Huzinaga basis[136] for beryllium by augmenting. Subsequently, Yeager and coworkers[132] showed that this basis set is somewhat inadequate for this resonance using their technique and the basis set containing at least $14p$ functions is much more reliable. It is also noteworthy that additional diffused functions must be added to the standard basis sets to describe accurately the electronic structure of the metastable state and to represent adequately the MSES where the absorbing potential is introduced in the peripheral part of the target. Therefore, we have initially chosen $14s11p$ basis set and augmented the p-type function with a view to account for the diffuse nature of the resonances. The augmentation in p-type functions is done by multiplying the factor $1/2.26^n$ to the most diffused function for $n = 1, 2$, and 3 to obtain $14s14p$ basis. Using this basis θ_0-trajectories of ^2P Be^- from different orders of dilated electron propagator are plotted in Figs. 4.4, 4.5, and 4.6.

From the figures, it is clearly seen that no improvement is observed after applying second order and third order dilated electron propagators. Whatever, McCurdy et al.[109] mentioned that simple SCF theory can provide appropriate results in characterizing shape resonances. This may be the reason that no discernible change is observed after applying higher order dilated electron propagators. The resonance energy and the width obtained from this calculation are 0.76 eV and 0.39 eV. However, the calculated results also vary depending on the type of basis sets. So to

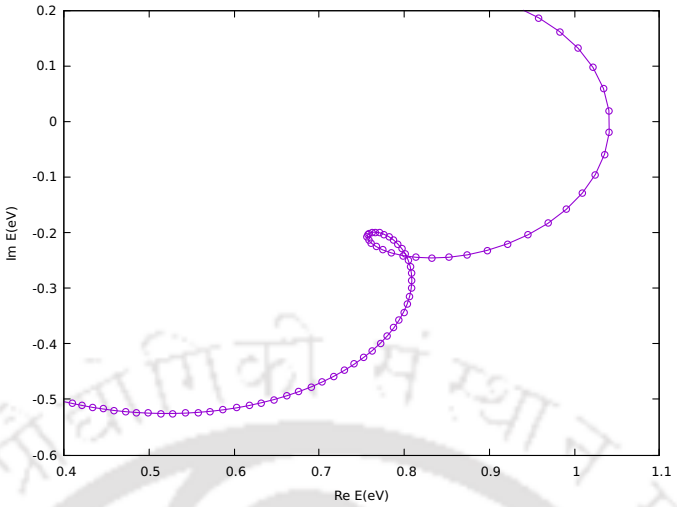

FIGURE 4.4: θ_0-trajectory of ^2P Be^- shape resonance at x_0=4.5 using $14s14p$ basis applying bivariational SCF-MSES (ZoDEP-MSES).

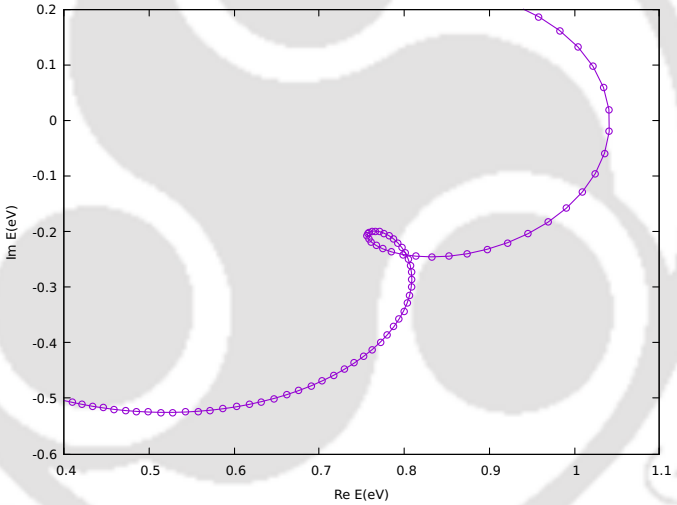

FIGURE 4.5: θ_0-trajectory of ^2P Be^- shape resonance at x_0=4.5 using $14s14p$ basis applying SoDEP-MSES.

make the calculated results more reliable we have done more calculations by using different basis sets. First, we have augmented the previous $14s14p$ basis by adding one more p-type function applying the same procedure to get $14s15p$ basis. Again, we have also used the basis set aug-cc-pVTZ+5s5p which was used by Yeager and coworkers[59, 133]. The θ_0-trajectories using these basis sets are plotted in the figures from 4.7 to 4.12. The resonance energies and widths obtained by using the

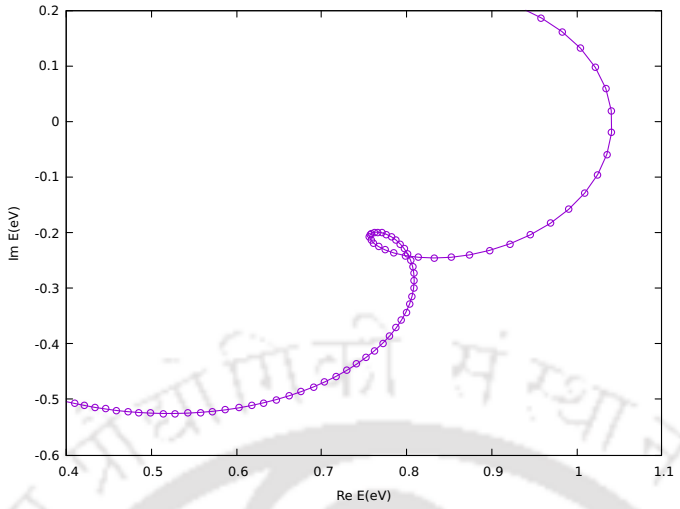

FIGURE 4.6: θ_0-trajectory of ^2P Be^- shape resonance at x_0=4.5 using $14s14p$ basis applying ToDEP-MSES.

mentioned basis sets and the results from other theoretical methods are presented in Table 4.2.

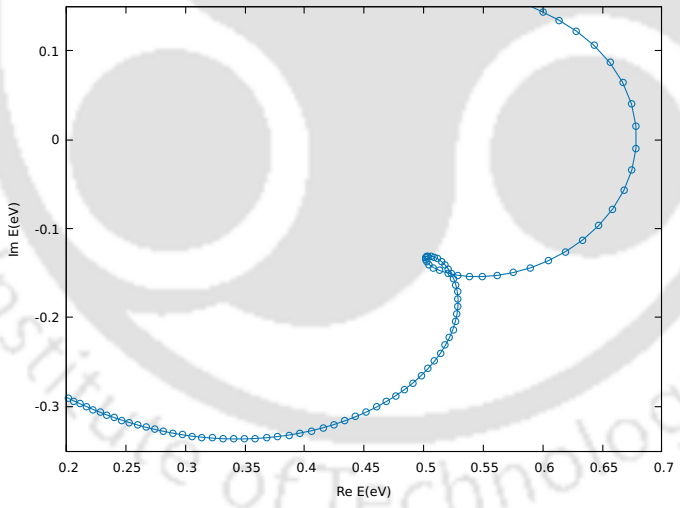

FIGURE 4.7: θ_0-trajectory of ^2P Be^- shape resonance at x_0=4.5 using $14s15p$ basis applying bivariational SCF-MSES (ZoDEP-MSES).

There is no experimental result available for ^2P Be^- shape resonance to compare our findings exactly. However, there is a large number of theoretical estimates in the literature which can be used to compare. The reported results available in the literature vary within 0.10-1.20 eV in the case of energy and 0.14-2.60 eV in the

Method	Energy (eV)	Width (eV)
Static exchange phase shift[137]	0.77	1.61
Static exchange plus polarizability phase shift[137]	0.20	0.28
Static exchange cross section[128]	1.20	2.60
Static exchange plus polarizability cross section[128]	0.16	0.14
S-matrix pole (X_α)[129]	0.10	0.15
Complex Δ SCF[109]	0.70	0.51
Singles, doubles and triples complex CI[130]	0.32	0.30
MCSCF/complex scaling[131]	0.31	0.49
M_1/complex scaling[49]	0.57	1.19
CAP/EOM-EA-CCSD/aug-cc-pVTZ+3s3p[75]	0.79	0.12
CMCSTEP(14s14p2d–2s2p3d CAS)[132]	0.79	0.68
CMCSTEP(14s14p5d–2s2p3d CAS)[132]	0.76	0.86
CMCSTEP(aug-cc-pVTZ+3s3p-2s2p3s3p3d CAS)[133]	0.73	0.74
CMCSTEP(aug-cc-pVTZ+5s5p-2s2p3s3p3d CAS)[133]	0.74	0.78
Stabilization method/EOM-EA-CCS[134]	0.33	0.40
CAP/EP-CASSCF/[14s,11p][79]	0.59	0.28
CAP/PP-CASSCF[14s,11p][83]	0.73	0.15
Results from bi-orthogonal dilated electron propagator[14s11p][102]		
Zeroth order	0.62	1.00
quasiparticle second order	0.61	1.00
Second order	0.48	0.82
quasiparticle third order	0.54	0.82
OVGF third order	0.54	0.78
Third order	0.53	0.85
ZoDEP-MSES/SoDEP-MSES/ToDEP-MSES [14s14p] (This work)	0.76	0.39
ZoDEP-MSES/SoDEP-MSES/ToDEP-MSES [14s15p] (This work)	0.50	0.26
ZoDEP-MSES/SoDEP-MSES/ToDEP-MSES [aug-cc-pVTZ+5s5p] (This work)	0.53	0.29

TABLE 4.2: Energy and Width of ^2P Be^- shape resonance.

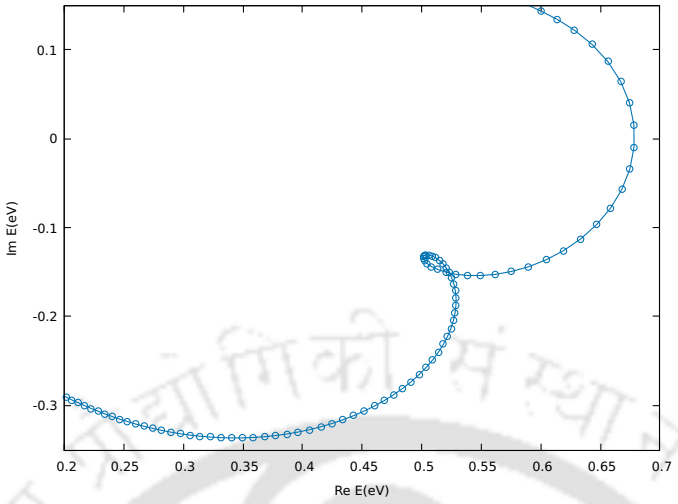

FIGURE 4.8: θ_0-trajectory of ^2P Be^- shape resonance at x_0=4.5 using $14s15p$ basis applying SoDEP-MSES.

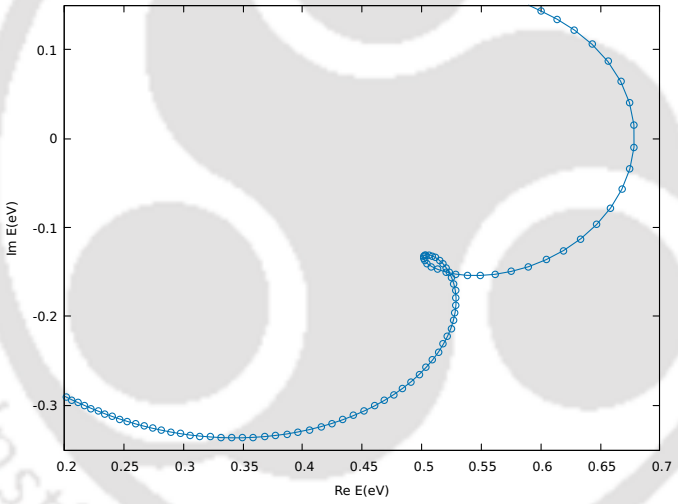

FIGURE 4.9: θ_0-trajectory of ^2P Be^- shape resonance at x_0=4.5 using $14s15p$ basis applying ToDEP-MSES.

case of width. The energy value obtained by using $14s14p$ basis set is comparable to most of the previous estimates[75, 83, 109, 132, 133, 137]. Significantly, the resonance energies and widths obtained by using $14s15p$ and aug-cc-pVTZ+5s5p are very close to the recent estimate by using the CAP/EP-CASSCF method[79]. From the above discussion, it is also observed that it is required to add more diffused functions in the standard basis sets that are best for other methods like CS or CAP

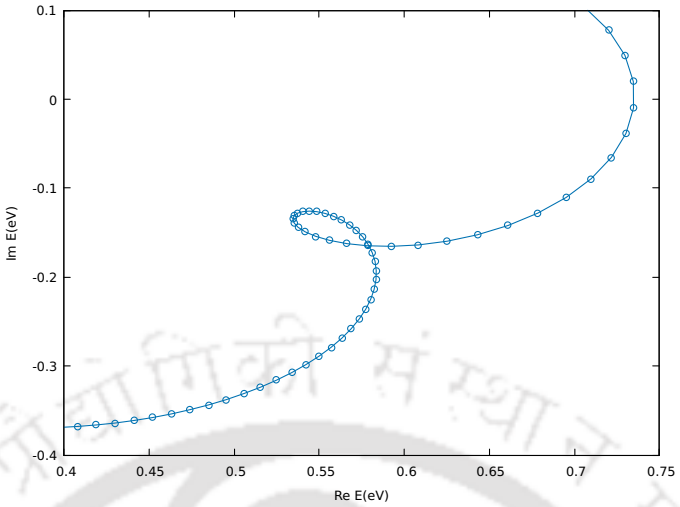

FIGURE 4.10: θ_0-trajectory of ^2P Be^- shape resonance at x_0=4.5 using aug-cc-pVTZ+5s5p basis applying bivariational SCF-MSES (ZoDEP-MSES).

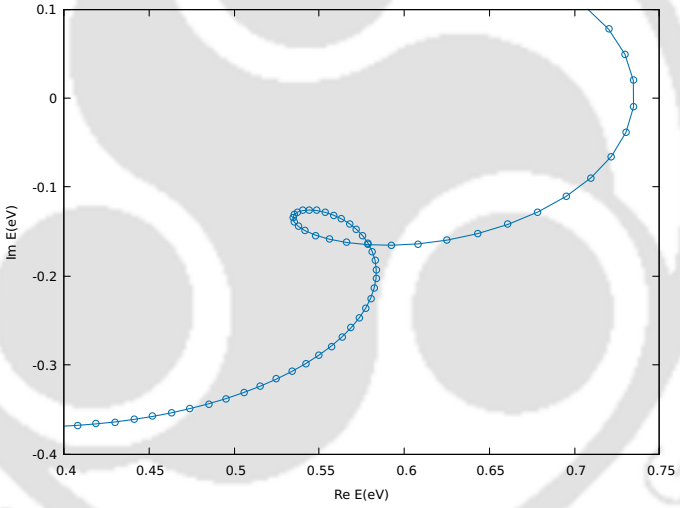

FIGURE 4.11: θ_0-trajectory of ^2P Be^- shape resonance at x_0=4.5 using aug-cc-pVTZ+5s5p basis applying SoDEP-MSES.

in describing the shape resonances while using the MSES method.

4.3 Conclusion

In this work, we have applied the electron propagator up to the third order in conjunction with MSES to investigate the ^{2}S Be^+1s^{-1} Auger and ^2P Be^- shape

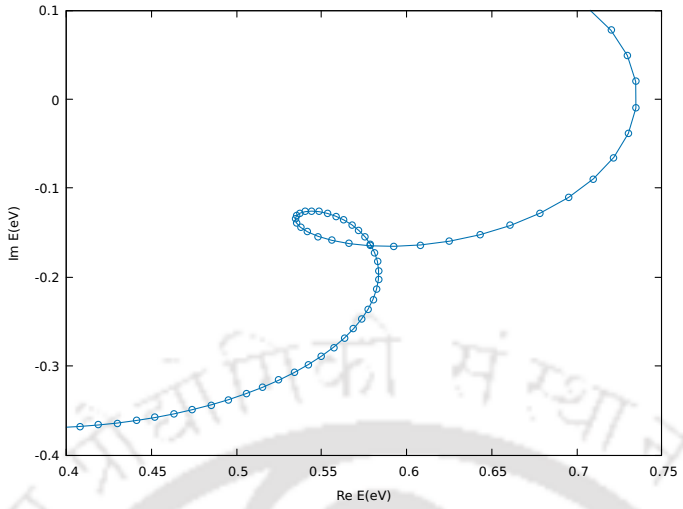

FIGURE 4.12: θ_0-trajectory of ^2P Be^- shape resonance at x_0=4.5 using aug-cc-pVTZ+5s5p basis applying ToDEP-MSES.

resonances. MSES method was developed by our group in studying the problems of quantum dynamics and, here, we have applied this method to characterize the Auger and shape resonances in Be. The results obtained from this calculation are in good agreement with experimental results and other theoretically calculated results available in the literature as portrayed in the tables. The application of dilated electron propagator reflects the inclusion of correlation and relaxation effects in the case of Auger resonance although it shows no major role in the case of shape resonance. This may be due to the fact that shape resonance can be characterized well at bivariational level itself with energy value comparable with other calculated results earlier. Thus, the MSES method has been proven to be an efficient method in characterizing electron scattering resonances. From this study, it is also clear that to get an efficient result by using MSES it is important to augment the basis sets. This is due to the fact that the application procedure of MSES is very similar to that of CAP where the scaling of resonance parameters is done outside the interaction region. Our group is working to implement this efficient method with other post SCF methods.

Chapter 5

Study of Effects of Diffused Basis Functions in Characterizing Electron Molecule Scattering Shape Resonances Using Modified Smooth Exterior Scaling

In this chapter, we have characterized the effect of additional diffused functions in studying shape resonances. The MSES method is applied to uncover the resonances. The study of shape resonances of some simple molecular systems, i.e., N_2^-, CO^-, F_2^- etc. is effective at bivariational SCF[109], therefore, we have done our characterization at that level only. Through this study, it can be clearly seen that the additional diffused functions play an important factor in the accurate calculation of resonance position and width.

5.1 Introduction

Quantum mechanically, resonances are the metastable states of a system that belong to the continuum part of the spectrum with wave functions that are not L^2-integrable. Using the outgoing boundary conditions the resonance wave function or Siegert wave function can be converted into the following form

$$\psi(x,t) = e^{-iEt/\hbar}\phi_R(x) = e^{-\Gamma t/2\hbar}e^{-iE_R t/\hbar}\phi_R(x) \tag{5.1}$$

where $\phi_R(x)$ is the bound state wave function in the interaction region and E_R and Γ represent the resonance position and width respectively. Thus, the resonances can be obtained as the solution of Schrödinger equation with complex eigenvalues, $E_{res} = E_R - i\frac{\Gamma}{2}$. The Γ is inversely proportional to the lifetime of the resonance state[2, 6, 138].

In an electron-molecule scattering experiment, an incoming particle (i.e. electron) with a specific energy collides with a molecular target and combines with the target producing a metastable state, transient state, temporary bound state, or resonance state. The quasi-bound nature of these states encouraged the theoreticians to introduce the techniques that can be used to solve by applying bound state-based methods. Different techniques used to calculate the resonance parameters in terms of bound state methods have been discussed in Chapter 1.

In this work, we have tried to study the effect of additional diffused functions in characterizing the resonance position and width by applying MSES[43]. Different studies of the same type have been done earlier by different researchers by applying CS[55–57] and CAP[74]. We have investigated the $^2\Pi_g$ N_2^-, $^2\Pi$ CO^- and $^2\Pi_g$ $C_2H_2^-$ shape resonances applying bivariational SCF method[46]. This method has been

successfully applied to study the shape resonances in atomic and molecular systems. They dilated the Hamiltonian by applying the CS method, but in the present work, the dilation has been done by applying MSES. McCurdy et al.[109] mentioned that the molecular shape resonances of some familiar systems (N_2^-, CO^-, F_2^-, etc.) can be characterized at the bivariational SCF level itself. Therefore, we have characterized the resonance positions and widths of the above mentioned systems up to bivariational SCF level only. The mathematical formulation of the method has been discussed in Chapter 2.

This chapter is organized as follows. In section 5.2 we present and compare the results obtained from our calculations and the experimental and theoretical results of others. In section 5.3, a summary of our findings is presented.

5.2 Results and Discussion

In this section, we present the effects of diffused basis functions observed in studying the e-molecule scattering shape resonances. We have characterized the resonance energies and widths of $^2\Pi_g$ N_2^-, $^2\Pi$ CO^- and $^2\Pi_g$ $C_2H_2^-$ shape resonances using different types of basis sets obtained by augmenting the standard basis set. These isoelectronic systems have been frequently used to test the effectiveness of different theoretical techniques in describing different molecular shape resonances quantitatively and qualitatively.

In this calculation, an augmented correlation-consistent polarized valence double zeta Gaussian basis set (aug-cc-pVDZ) centered at the origin is employed on each atom of studied molecules. In characterizing shape resonances, the augmentation of the standard basis set by adding more diffused basis functions is required to describe accurately the electronic structure of the metastable state[132]. Also, the additional

diffused functions become more important while applying the MSES method as the absorbing potential is introduced in the peripheral part of the molecule. The augmentations have been done by multiplying the most diffused functions of the type s, p, and d by the factor $\frac{1}{2^n}$ where n is an integer that starts from 1. Thus, the generated basis sets will be termed as aug-cc-pVDZ+n_ssn_ppn_dd where n_s, n_p, and n_d refer to the number of additional diffused functions added to the respective type of functions. The MSES parameter λ is used as 10.00 a.u. for all the systems. The same value of λ has been used in various calculations where the same method is applied[51, 88].

In Chapter 3, we used the basis set aug-cc-pCVDZ by augmenting and obtained an efficient result as compared to experimental and other theoretically calculated results. The aug-cc-pCVXZ series of basis sets, where X=D,T,Q,5,..etc, which are known as augmented correlation-consistent polarized valence basis sets are used for accurately describing core and core-valence correlation effects. These are also used to study a number of standard test cases. These series of basis sets are derived from aug-cc-pVXZ series by adding different number of basis functions in the usual pattern[139]. The results obtained from that calculation will be used to compare the results obtained from the present calculation with the equal number of added basis functions, i.e., aug-cc-pVDZ+5s5p.

5.2.1 $^2\Pi_g$ shape resonance in N_2^-

The electron scattering in the N_2 molecule is a well-studied problem both experimentally and theoretically. In this section, we have characterized the effect of diffused functions in the study of $^2\Pi_g$ N_2^- shape resonance by using different basis sets generated by augmenting. This $^2\Pi_g$ state in the N_2 molecule is the result of the addition

Basis set	Energy (eV)	Width (eV)
aug-cc-pVDZ+3s3p	–[c]	–[c]
aug-cc-pVDZ+4s	–[c]	–[c]
aug-cc-pVDZ+4p	1.964	0.294
aug-cc-pVDZ+4s4p	1.964	0.294
aug-cc-pVDZ+4s5p/5s5p	2.136	0.394
aug-cc-pVDZ+4s4p1d	1.955	0.295
aug-cc-pVDZ+4s6p/4s7p	–[c]	–[c]
aug-cc-pVDZ+4s8p	2.258	0.473
aug-cc-pVDZ+4s9p	2.266	0.479
aug-cc-pVDZ+4s10p	–[c]	–[c]
Experiment	2.32	0.41

[c]No well stabilized stationary point is observed.

TABLE 5.1: Energy and Width of $^2\Pi_g$ N_2^- shape resonance using different basis sets.

of an electron to the π_g LUMO of the ground state of the neutral N_2 molecule. The resultant electronic configuration is $(core)^4(1\sigma_g)^2(1\sigma_u)^2(2\sigma_g)^2(1\pi_u)^4(n\pi_g)^1$. To calculate resonance energy and width, the equilibrium bond length of the N_2 molecule 1.09 Å has been used. The N_2 molecule is placed along the x-axis symmetrical to the origin at (± 0.545 Å, 0.0, 0.0). The optimal value of x_0 has been chosen as 4.5 a.u. We have employed the basis set aug-cc-pVDZ and thereafter start adding the different number of diffused functions. We do not get any stationary point for the basis sets aug-cc-pVDZ+n_ssn_pp for $n_s = n_p$=0,1,2,3. We can see the first well-stabilized stationary point for the basis set aug-cc-pVDZ+4p, but not for aug-cc-pVDZ+4s. The θ_0-trajectories for different basis sets for which well stabilized stationary points are observed are plotted in Fig. 5.1 The resonance energies and widths obtained for different basis sets are collected in Table 5.1.

From Table 5.1, it is also observed that adding four s-type functions to the basis aug-cc-pVDZ+4p does not change the value of energy and width. Both the energies and widths obtained from the basis sets aug-cc-pVDZ+4p and aug-cc-pVDZ+4s4p

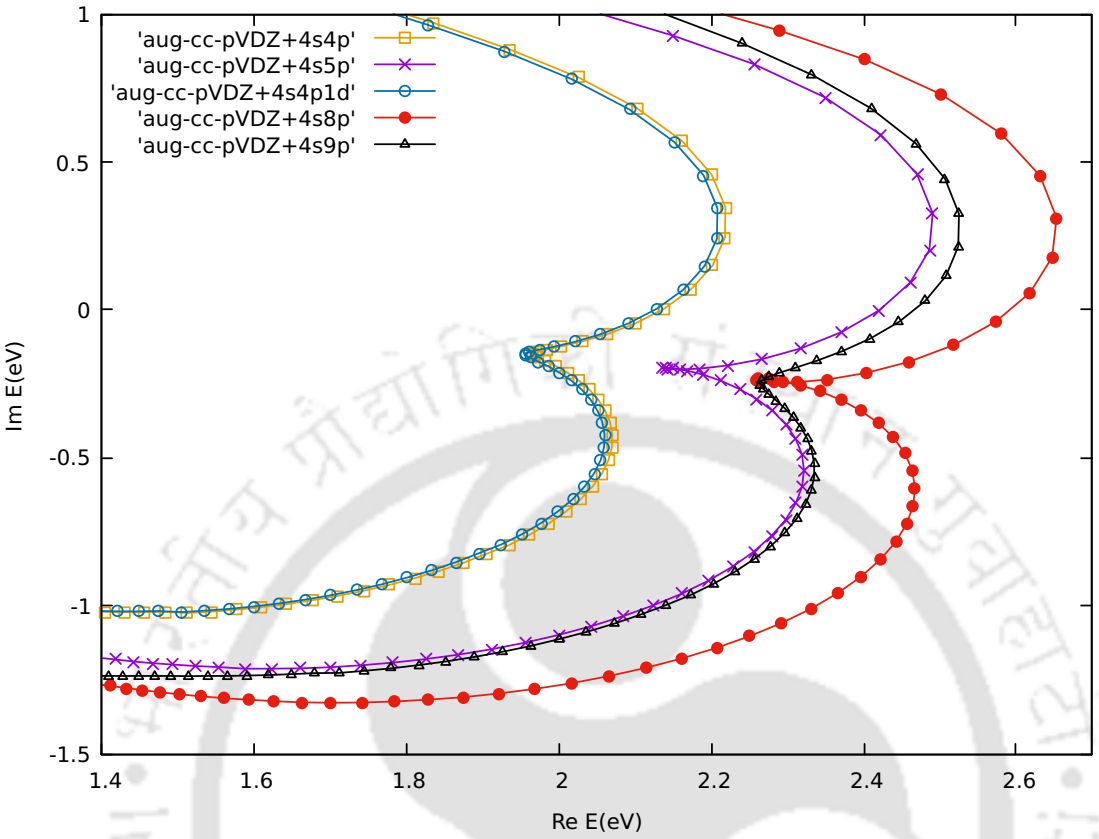

FIGURE 5.1: θ_0-trajectories of $^2\Pi_g$ N_2^- shape resonance by using different basis sets generated by augmenting the basis aug-cc-pVDZ applying bivariational SCF-MSES at x_0=4.5.

are the same i,e., 1.96 eV and 0.29 eV respectively. This indicates that the additional s-type functions added have no impact in characterizing the molecular shape resonances.

However, the crucial role of the p-type function in characterizing $^2\Pi_g$ N_2^- shape resonance is very clearly observed. With the addition of a diffused p-type function, a major change in both energy and width is seen. This can be understood by analyzing the results from the basis sets aug-cc-pVDZ+4s4p and aug-cc-pVDZ+4s5p, where the addition of one p-type function leads to a change of 0.172 eV in energy and 0.10 eV in width.

Like in the case of the s-type function, the addition of a diffused d-type function also

does not have any major impact in this study. By adding one d-type function to the basis aug-cc-pVDZ+4s4p, the change in energy and width observed for the basis aug-cc-pVDZ+4s4p1d are 0.011 eV and 0.001 eV respectively. Also, the addition of the d-type function may provide some polarization and will not give any contribution to the $\pi^\star$ symmetry which is required to describe $^2\Pi_g$ N_2^- shape resonance.

The results obtained by using the basis aug-cc-pCVDZ+5s5p in our previous work in Chapter 3 and aug-cc-pVDZ+5s5p from the present work are the same. This indicates that core and core-valence correlation effects have no crucial role in studying shape resonances in $^2\Pi$ states.

Now, to check the basis set convergence, we have added more p-type functions to the basis set on each nitrogen atom. With the addition of subsequent p-type functions both the resonance energy and width are increased. Again, we do not observe any well-stabilized stationary points for basis sets aug-cc-pVDZ+4s6p and aug-cc-pVDZ+4s7p. The resonance energies and widths obtained for basis sets aug-cc-pVDZ+4s8p and aug-cc-pVDZ+4s9p are very close to each other and no well-stabilized stationary point is observed for basis aug-cc-pVDZ+4s10p. This indicates that the basis set convergence is reached. The resonance energy and width obtained for basis aug-cc-pVDZ+4s9p are 2.266 eV and 0.479 eV respectively which are very close to the experimental and other theoretically calculated results.

5.2.2 $^2\Pi$ shape resonance in CO^-

Although the $^2\Pi$ CO^- shape resonance is isoelectronic to $^2\Pi_g$ N_2^- shape resonance, the former is less frequently studied. From the available data in the literature, it is observed that, in the case of resonance energy, most of the theoretical values calculated are almost higher than the experimental value (1.50 eV) as in the case of N_2^-.

Method	Energy (eV)	Width (eV)
Experiment	2.32	0.41
Linear algebric method[111]	2.13	0.31
Static exchange R-matrix[112]	2.15	0.34
Stabilization method[113]	2.44	0.32
Boomerang model[114]	1.91	0.54
Complex SCF[115]	3.19	0.44
Second order dilated electron propagator(real SCF)[116]	2.14	0.26
CAP-FSMRCC[72]	2.52	0.39
EOM-CCSD[73]	2.07	0.42
dp-CAP-EOM-EA-CCSD($r_j^{CAP} \neq 0$)[74]	2.57	0.26
rm-CAP-EOM-EA-CCSD($r_j^{CAP} \neq 0$)[76]	2.50	0.35
rm-CAP-EOM-EA-CCSD($r_j^{CAP} = 0$)[76]	2.53	0.32
EOM-EA-CCSD[66]	2.54	0.52
MCSCF-CAP[79]	3.12	0.31
CAP/EA-ADC(3)[117]	2.54	0.40
CAP-MRCIS(5,8)/aug-cc-pVTZ+gh[3s3p3d][81]	3.06	0.40
CAP/PP-CASSCF[83]	3.83	0.25
Bivariational SCF-MSES (From Chapter 3)	2.14	0.39
SoDEP-MSES (From Chapter 3)	2.14	0.39
Results from biorthogonal dilated electron propagator[58]		
Zeroth order, quasi particle second order and quasi particle diagonal 2ph-TDA	2.12	0.19
Second order	2.11	0.18
Diagonal 2ph-TDA	2.12	0.18
Quasi-particle/OVGF third order	2.11	0.18
Third order	2.11	0.18
This work/aug-cc-pVDZ+4s9p	2.266	0.479

TABLE 5.2: Energy and Width of $^2\Pi_g$ N_2^- shape resonance from different methods.

The ground state electronic configuration of the CO molecule is $1\sigma^2 2\sigma^2 3\sigma^2 4\sigma^2 5\sigma^2 1\pi^4$. The $^2\Pi$ state of CO^- is generated by adding an electron to the 2π LUMO of the $^1\Sigma^+$ ground state of the neutral CO molecule. To study the $^2\Pi$ CO^- shape resonance, the equilibrium bond length of CO molecule 1.128 Å is used. The CO molecule is placed along the x-axis symmetrical to the origin at (± 0.564 Å, 0.0, 0.0). The optimal value of x_0 has been chosen as 3.3 a.u. Different basis sets obtained by augmenting as described above are employed. We do not observe well-stabilized stationary

points for the basis sets aug-cc-pVDZ+n_ssn_pp for n=1 to 4. We can get the first well-stabilized stationary point for aug-cc-pVDZ+5p but not for aug-cc-pVDZ+5p as in the case of $^2\Pi_g$ N_2^- shape resonance. The θ_0-trajectories for different augmented basis sets for which well-stabilized stationary points are observed are plotted in Fig. 5.2.

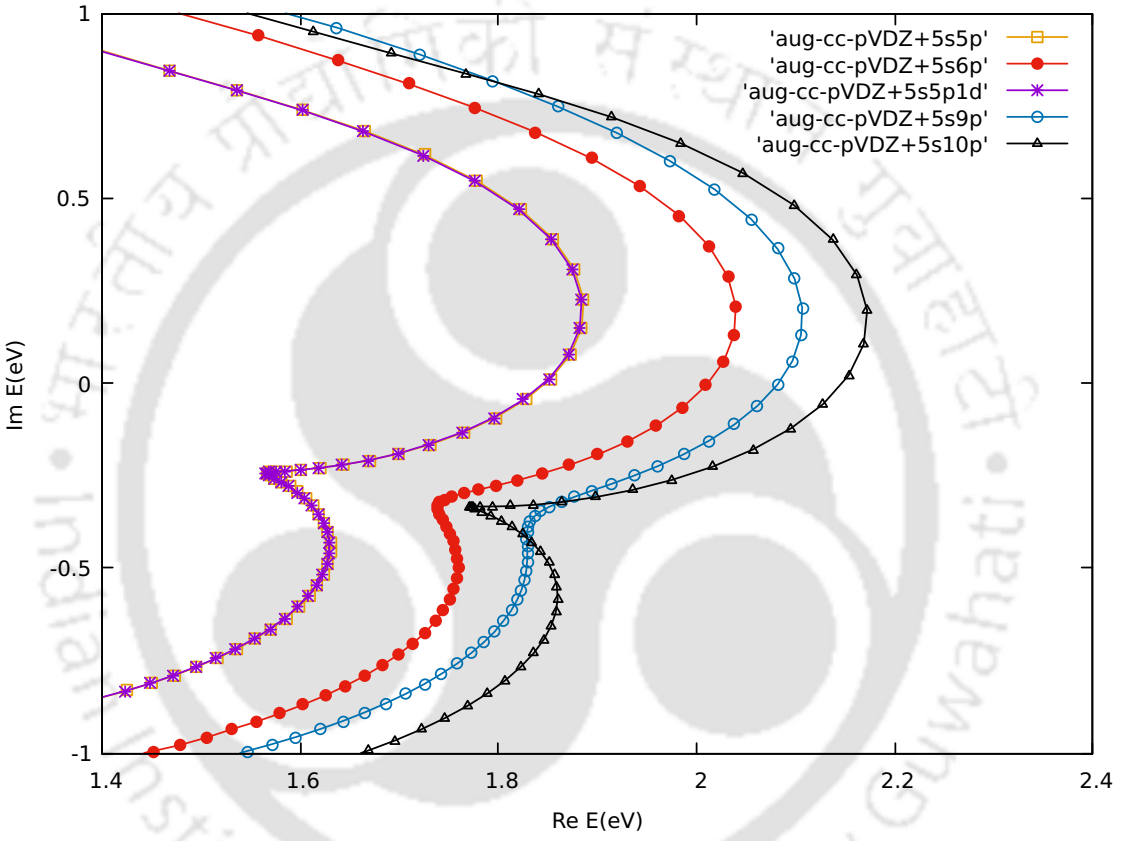

FIGURE 5.2: θ_0-trajectory of $^2\Pi$ CO^- shape resonance using different basis sets generated by augmenting the basis aug-cc-pVDZ applying bivariational SCF-MSES at x_0=3.3 a.u.

The resonance energy and width obtained from the θ_0-trajectories are collected in Table 5.3. In $^2\Pi$ CO^- shape resonance also, the same effect is observed with the addition of diffused functions as in the case of N_2^-. We do not observe any change in the values after adding five s-type functions to the basis aug-cc-pVDZ+5p generating aug-cc-pVDZ+5s5p which indicates that the additional s-type function has no impact. After adding one p-type function to aug-cc-pVDZ+5s5p, we can see

Basis set	Energy (eV)	Width (eV)
aug-cc-pVDZ+4s4p	–[c]	–[c]
aug-cc-pVDZ+5s	–[c]	–[c]
aug-cc-pVDZ+5p	1.566	0.491
aug-cc-pVDZ+5s5p	1.566	0.491
aug-cc-pVDZ+5s6p	1.739	0.664
aug-cc-pVDZ+5s5p1d	1.565	0.493
aug-cc-pVDZ+5s7p/5s8p	–[c]	–[c]
aug-cc-pVDZ+5s9p	1.858	0.667
aug-cc-pVDZ+5s10p	1.795	0.591
aug-cc-pVDZ+5s11p	–[c]	–[c]
Experiment[118]	1.50	0.40

[c]No well stabilized stationary point is observed.

TABLE 5.3: Energy and Width of $^2\Pi$ CO^- shape resonance using different basis sets generated by augmentation.

the change in energy is 0.173 eV and in width is 0.173 eV which proves the crucial role of additional diffused p-type functions. The addition of one d-type function to the basis aug-cc-pVDZ+5s5p generating aug-cc-pVDZ+5s5p1d leads to a change of 0.001 eV in energy and 0.002 eV in width which means that the extra d-type function added has no major role. Again, the resonance energy and width obtained by using aug-cc-pVDZ+5s5p are 1.57 eV and 0.49 eV respectively which is the same as obtained by using the basis aug-cc-pCVDZ+5s5p. This indicates that the core and core-valence correlation effects have no role in the case of $^2\Pi$ CO^- shape resonance too.

We have also studied the basis set convergence for $^2\Pi$ CO^- shape resonance. For this, more p-type functions are added gradually on both the carbon and oxygen atoms to reach the expansion limit. We do not observe well-stabilized stationary points for the basis sets aug-cc-pVDZ+5s7p and aug-cc-pVDZ+5s8p. The resonance energy and width decrease while one p-type function is added to aug-cc-pVDZ+5s9p to generate aug-cc-pVDZ+5s10p and no well-stabilized stationary point is observed for basis aug-cc-pVDZ+5s11p. This indicates that the basis set convergence is reached.

Method	Energy (eV)	Width (eV)
Experiment[118]	1.50	0.40
Boomerang model[119]	1.52	0.80
Close coupling method[120]	1.75	0.28
Second order dilated electron propagator(real SCF)[121]	1.71	0.10
EOM-CCSD[73]	1.32	0.12
dp-CAP-EOM-EA-CCSD($r_j^{CAP} \neq 0$)[74]	1.98	0.59
rm-CAP-EOM-EA-CCSD($r_j^{CAP} \neq 0$)[76]	2.01	0.60
rm-CAP-EOM-EA-CCSD($r_j^{CAP} = 0$)[76]	2.09	0.61
EOM-EA-CCSD[66]	2.04	1.03
MCSCF-CAP[79]	1.28	0.32
CAP/EA-ADC(3)[117]	1.95	0.63
CAP/PP-CASSCF[83]	2.16	0.31
Bivariational SCF-MSES (From Chapter 3)	1.57	0.49
SoDEP-MSES (From Chapter 3)	1.49	0.50
Results from bi-orthogonal dilated electron propagator[58]		
Zeroth order, quasiparticle second order and quasiparticle diagonal 2ph-TDA	1.71	0.10
Second order	1.68	0.09
Diagonal 2ph-TDA	1.69	0.08
Quasi-particle third order and OVGF third order	1.65	0.14
Third order	1.65	0.14
This work/aug-cc-pVDZ+5s10p	1.795	0.591

TABLE 5.4: Energy and Width of $^2\Pi$ CO^- shape resonance from different methods..

The resonance energy to basis aug-cc-pVDZ+5s10p is 1.795 eV and the width is 0.591 eV which is close to experimental results and comparable to other theoretically calculated results.

5.2.3 Comparison between the $^2\Pi_g$ N_2^- and $^2\Pi$ CO^- shape resonances

In this section, we would like to compare the resonance parameters obtained for $^2\Pi_g$ N_2^- and $^2\Pi$ CO^- shape resonances employing the same basis set aug-cc-pVDZ+5s5p.

System	Energy (eV)	Width (eV)
N_2^-	2.136	0.394
CO^-	1.566	0.491

TABLE 5.5: Energy and Width of $^2\Pi_g$ N_2^- and $^2\Pi$ CO^- shape resonances obtained using aug-cc-pVDZ+5s5p basis set.

The results are presented in Table 5.5. The same type of observation has been done by Pal and coworkers[73] and our results also follow the same trend. The resonance energy of N_2^- is 2.136 eV which is larger than the energy of CO^- shape resonance which is 1.566 eV. On the other hand, the width of N_2^- is lower than that of CO^-. This trend in the result is expected because the $^2\Pi$ CO^- shape resonance contains p-wave as well as d-wave which are not present in $^2\Pi_g$ N_2^- shape resonance. The polarization effects are the same in both systems. The potential energy barrier which is very important for the shape resonance is stronger in N_2^- than CO^-. Although the behavior of both systems is similar, the coupling between the partial waves is much stronger in the CO molecule.

5.2.4 $^2\Pi_g$ shape resonance in $C_2H_2^-$

The $^2\Pi_g$ $C_2H_2^-$ shape resonance is also well studied theoretically and experimentally. The $^2\Pi_g$ state of $C_2H_2^-$ is generated by adding an electron to the π_g LUMO of the $^1\Sigma_g^+$ ground state of the neutral C_2H_2 molecule. The resulting electronic configuration of the $^2\Pi_g$ state of $C_2H_2^-$ is $(core)^4(1\sigma_g)^2(1\sigma_u)^2(2\sigma_g)^2(1\pi_u)^4(n\pi_g)^1$. To estimate the resonance energy and width of $^2\Pi_g$ $C_2H_2^-$ shape resonance, we have used C-C bond length 1.2026 Å and C-H bond length 1.063 A^0. The C_2H_2 molecule is placed along the x-axis symmetrical to the origin. The optimal value of x_0 is 4.5 a.u. The basis set aug-cc-pVDZ is used in this system also. The basis set is further augmented to generate different bases as mentioned above. Here, the augmentation is done

only for carbon atoms only. No well-stabilized stationary point is observed for basis sets aug-cc-pVDZ+n_ssn_pp for $n_s = n_p$=0,1,2,3 and aug-cc-pVDZ+4s. We can see the first well-stabilized stationary point for the basis set aug-cc-pVDZ+4p. The θ_0-trajectories for which stationary points are observed are plotted in Fig 5.3. The resonance energy and width are presented in Table 5.6.

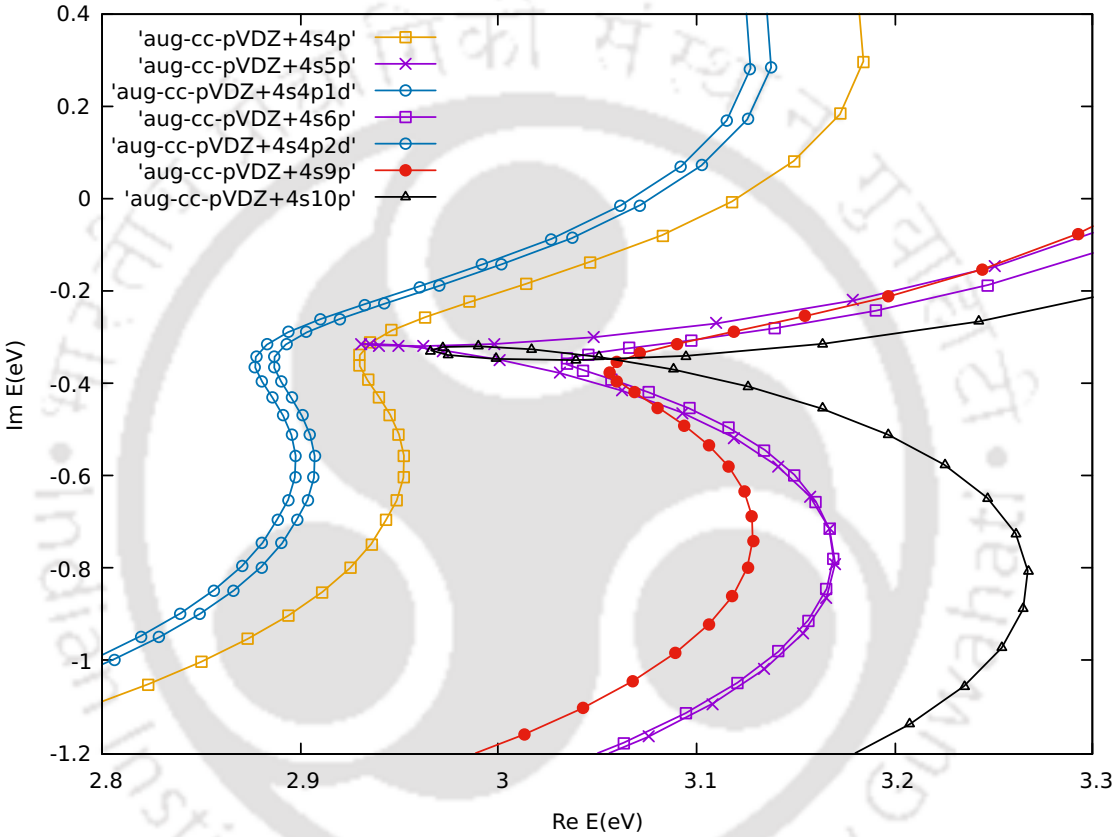

FIGURE 5.3: θ_0-trajectories of $^2\Pi_g$ $C_2H_2^-$ shape resonance using different basis sets generated by augmenting the basis aug-cc-pVDZ applying bivariational SCF-MSES at x_0=4.5.

In the case of $^2\Pi_g$ $C_2H_2^-$ shape resonance also, the same effect of diffused functions is observed as in the case of $^2\Pi_g$ N_2^- shape resonance. The addition of four s-type functions to the basis aug-cc-pVDZ+4p generating aug-cc-pVDZ+4s4p do not make any change in both energy and width value. We can observe a jump of 0.001 eV in energy and 0.09 eV in width after adding one p-type function to the basis aug-cc-pVDZ+4s4p to get aug-cc-pVDZ+4s5p. After adding one d-type function to the

Basis set	Energy (eV)	Width (eV)
aug-cc-pVDZ+3s3p	_[c]	_[c]
aug-cc-pVDZ+4s	_[c]	_[c]
aug-cc-pVDZ+4p	2.930	0.725
aug-cc-pVDZ+4s4p	2.930	0.725
aug-cc-pVDZ+4s5p	2.931	0.630
aug-cc-pVDZ+4s4p1d	2.887	0.733
aug-cc-pVDZ+4s6p	3.035	0.694
aug-cc-pVDZ+4s4p2d	2.877	0.732
aug-cc-pVDZ+4s7p/4s8p	_[c]	_[c]
aug-cc-pVDZ+4s9p	3.056	0.750
aug-cc-pVDZ+4s10p	2.966	0.658
aug-cc-pVDZ+4s11p	_[c]	_[c]
Experiment		
Trapped electron[140, 141]	1.8/1.85	...
Vibrational excitation[142]	2.60	>1.00
Dissociative attachment[143]	2.94±0.1	
Electron impact[144]	2.50	
Dissociative electron attachment[145]	2.95	

[c]No well stabilized stationary point is observed.

TABLE 5.6: Energy and Width of $^2\Pi_g$ $C_2H_2^-$ shape resonance using aug-cc-pVDZ basis set with different augmentations.

basis aug-cc-pVDZ+4s4p, we can see a decrease in energy value only by 0.043 eV and an increase in width by 0.008 eV. However, these changes do not make clear the study. So, to get clear a picture, we have added one more p-type and one more d-type function to the basis aug-cc-pVDZ+4s4p to get aug-cc-pVDZ+4s6p and aug-cc-pVDZ+4s4p2d basis sets respectively. The addition of one more p-type function (i.e. for basis aug-cc-pVDZ+4s6p) leads to a change of 0.105 eV in energy and 0.031 eV in width. But, the addition of one more d-type function (i.e. for basis aug-cc-pVDZ+4s4p2d) leads to a change of 0.053 eV in energy and 0.007 eV in width. From this observation, it is clear that the additional p-type function plays an important role in characterizing the $^2\Pi_g$ $C_2H_2^-$ shape resonance also.

Method	Energy (eV)	Width (eV)
Experiment		
Trapped electron[140, 141]	1.8/1.85	...
Vibrational excitation[142]	2.60	>1.00
Dissociative attachment[143]	2.94±0.1	
Electron impact[144]	2.50	
Dissociative electron attachment[145]	2.95	
Theoretical approaches		
CI[146]	3.29/2.92	1.10/1.10
EOM-CCSD[73]	2.61	0.76
dp-CAP-EOM-EA-CCSD($r_j^{CAP} \neq 0$)[74]	2.45	0.83
Results from bi-orthogonal dilated electron propagator[58]		
Zeroth order, quasiparticle second order and quasiparticle diagonal 2ph-TDA	2.58	0.23
Second order	2.46	0.19
Diagonal 2ph-TDA	2.49	0.20
Quasi-particle third order	2.51	0.21
OVGF third order and Third order	2.50	0.21
This work/aug-cc-pVDZ+4s10p	2.966	0.658

TABLE 5.7: Energy and Width of $^2\Pi_g$ $C_2H_2^-$ shape resonance from different methods.

For basis set convergence, we add gradually p-type functions on both the carbon atoms. No well-stabilized stationary point is obtained for basis sets aug-cc-pVDZ+4s7p and aug-cc-pVDZ+4s8p. From basis aug-cc-pVDZ+4s5p, with adding the p-type function, both resonance energy and width start increasing like in the case of $^2\Pi$ CO^- shape resonance. The resonance energy and width decrease for the basis aug-cc-pVDZ+4s10p and no well-stabilized stationary point is observed for basis aug-cc-pVDZ+4s11p. This shows the achievement of convergence results for basis aug-cc-pVDZ+4s10p where the resonance energy is 2.966 eV and the width is 0.658 eV. This result is very close to the experimental results obtained from dissociative attachment[143] and Dissociative electron attachment[145] and theoretically estimated values from CI[146].

5.3 Conclusion

In this work, we have studied the effect of diffused basis functions in the investigation of electron-molecule scattering shape resonances. From the study, it is observed that in characterizing the $^2\Pi$ shape resonances, the augmentation of the p-type functions has a very important role. However, the s- and d-type functions have negligible impact. This is due to the fact that in $^2\Pi_g$ N_2^-, $^2\Pi$ CO^- and $^2\Pi_g$ $C_2H_2^-$ shape resonances the LUMO orbitals are associated with p-type orbitals. Also, it is observed that core and core-valence correlation effects have no role in characterizing the $^2\Pi$ shape resonances in molecular systems. From this study of the effect of the basis sets it can be seen that the basis set convergence can be obtained by adding additional diffused p-type functions to standard basis sets. It can also be concluded, from this calculation, that additional diffused basis functions, especially p-type functions, are very important to calculate accurate resonance energy and width.

Chapter 6

Summary and Conclusions

This work involves the implementation of the MSES method to study the electron-atom and electron-molecule scattering resonances. This is the first time that the MSES has been applied in three-dimensional many-body electron systems. MSES converts the divergent resonance wave functions into square integrable ones thereby making the study of temporary bound states (resonance states) amenable to bound state electronic structure methods. This type of study needs modification of existing electronic structure codes. In this study, we apply the bivariational SCF (complex scaled by MSES) method to calculate the complex resonance energy, $E = E_R - i\frac{\Gamma}{2}$. The resonance parameters obtained from bivariational SCF level are treated using the dilated electron propagator up to the third order incorporating the higher order relaxation and correlation effects.

In standard quantum mechanics, the Hamiltonian is Hermitian, and hence cannot obtain complex eigenvalues. As a result, the resonances stay hidden in the continuum part of the Hamiltonian. These resonances can be revealed by applying various approaches discussed in Chapter 1. This chapter also includes a brief description of resonance metastable states and their importance.

In the next chapter, we have discussed about the mathematical formulation of the MSES method in dilating the physical Hamiltonian. In this method, a universal problem independent reflection free CAP is added to the Hamiltonian to make the dilation transformation generating an effective Hamiltonian. A graphical method to obtain the resonance position and width has also been discussed.

The bivariational SCF-MSES has been applied to study the $^2\Pi_g$ N_2^- and $^2\Pi$ CO^- shape resonances in chapter 3. With the aim of improving the results, we have used dilated electron propagator up to second order SoDEP-MSES). After applying SoDEP-MSES, we do not observe any improvement in the case of $^2\Pi_g$ N_2^- shape resonance, however, in the case of $^2\Pi$ CO^- shape resonances the resonance position shows improvement. From this observation, the MSES method has been proven to be quite reliable and effective in investigating molecular shape resonances.

In the next chapter, the dilated electron propagator has been used up to third order (ToDEP-MSES) to investigate the Auger and shape resonances in Be. Using the basis $14s11p$, which was used earlier by various researchers, the energy position obtained for $1s^{-1}$ Auger hole in Be is 123.66 eV (ToDEP-MSES) which is very close to the experimental result and the width is 0.38 eV. Along with this, the ^2P Be^- shape resonance has also been studied. The resonance energy and the width obtained by using $14s14p$ basis obtained by augmenting $14s11p$ are 0.76 eV and 0.39 eV respectively. Further, to make this calculation more effective two more basis sets have been used, $14s15p$ obtained by adding one more p-type function to $14s14p$ and aug-cc-pVTZ+5s5p. The results obtained from these two bases are very close to each other. From this, it is observed that the addition of diffused functions to the standard basis sets is required to calculate accurate resonance position and width.

In the final work, we have characterized the effect of additional diffused functions in studying the molecular shape resonances. We have investigated well known $^2\Pi_g$ N_2^-,

$^2\Pi$ CO^- and $^2\Pi_g$ $C_2H_2^-$ shape resonances applying bivariational SCF. In this study, different basis sets have been generated by augmenting the basis aug-cc-pVDZ by multiplying the most diffused functions of type s, p, and d by the factor $\frac{1}{2^n}$ where n is an integer that starts from 1. We have also studied the basis set convergence for these molecular shape resonances.

From this study, it is observed that the MSES is an effective method in characterizing the Auger and shape resonances in atomic and small molecular systems. Our group is working to apply this effective method along with other *ab initio* methods like DFT, couple cluster, MCSCF, etc.

References

(1) Mishra, M. K.; Venkatnathan, A. *Int. J. Quantum Chem.* **2002**, *90*, 1334–1347.

(2) Klaiman, S.; Gilary, I. In *Adv. Quantum Chem.* Elsevier: 2012; Vol. 63, pp 1–31.

(3) Hazi, A. U.; Taylor, H. S. *Phys. Rev. A* **1970**, *1*, 1109.

(4) Schulz, G. J. *Rev. Mod. Phys.* **1973**, *45*, 378.

(5) Moiseyev, N. *Phys. Rep.* **1998**, *302*, 212–293.

(6) Moiseyev, N., *Non-Hermitian Quantum Mechanics*; Cambridge University Press: 2011.

(7) Donnelly, R. A.; Simons, J. *J. Chem. Phys.* **1980**, *73*, 2858–2866.

(8) Bardsley, J.; Biondi, M. In *Adv. At. Mol. Phys.* Elsevier: 1970; Vol. 6, pp 1–57.

(9) Massey, H., *Negative Ions*; Cambridge University Press: 1976.

(10) Aflatooni, K.; Gallup, G. A.; Burrow, P. *J. Phys. Chem. A* **1998**, *102*, 6205–6207.

(11) Boudaıffa, B.; Cloutier, P.; Hunting, D.; Huels, M. A.; Sanche, L. *Science* **2000**, *287*, 1658–1660.

(12) Li, X.; Sevilla, M. D.; Sanche, L. *J. Am. Chem. Soc.* **2003**, *125*, 13668–13669.

(13) Huels, M. A.; Boudaïffa, B.; Cloutier, P.; Hunting, D.; Sanche, L. *J. Am. Chem. Soc.* **2003**, *125*, 4467–4477.

(14) Tonzani, S.; Greene, C. H. *J. Chem. Phys.* **2006**, *124*.

(15) Simons, J. *Acc. Chem. Res.* **2006**, *39*, 772–779.

(16) Li, Z.; Cloutier, P.; Sanche, L.; Wagner, J. R. *J. Am. Chem. Soc.* **2010**, *132*, 5422–5427.

(17) Cheng, H.-Y.; Chen, C.-W. *J. Phys. Chem. A* **2011**, *115*, 10113–10121.

(18) Renjith, B; Bhowmick, S.; Mishra, M. K.; Sarma, M. *J. Phys. Chem. A* **2011**, *115*, 13753–13758.

(19) Bhowmick, S.; Mishra, M. K.; Sarma, M., et al. *J. Chem. Phys.* **2012**, *137*.

(20) Bhaskaran, R.; Sarma, M. *J. Phys. Chem. A* **2015**, *119*, 10130–10136.

(21) Tripathi, D.; Dutta, A. K. *J. Phys. Chem. A* **2019**, *123*, 10131–10138.

(22) Kumari, B.; Huwaidi, A.; Robert, G.; Cloutier, P.; Bass, A. D.; Sanche, L.; Wagner, J. R. *J. Phys. Chem. B* **2022**, *126*, 5175–5184.

(23) Corkum, P. á.; Krausz, F. *Nature Phys.* **2007**, *3*, 381–387.

(24) Strelkov, V *Phys. Rev. Lett.* **2010**, *104*, 123901.

(25) Bressler, C.; Chergui, M. *Chem. Rev.* **2004**, *104*, 1781–1812.

(26) Liakhou, G; Paoloni, S; Bertolotti, M *J. Appl. Phys.* **2004**, *96*, 4219–4224.

(27) Chu, S.-I.; Telnov, D. A. *Phys. Rep.* **2004**, *390*, 1–131.

(28) Ullrich, J.; Rudenko, A.; Moshammer, R. *Annu. Rev. Phys. Chem.* **2012**, *63*, 635–660.

(29) Sajeev, Y; Moiseyev, N *Phys. Rev. B* **2008**, *78*, 075316.

(30) Genkin, M.; Lindroth, E. *Phys. Rev. B* **2010**, *81*, 125315.

(31) Simons, J. *Int. J. Quantum Chem.* **1980**, *18*, 113–121.

(32) Taylor, H. S.; Hazi, A. U. *Phys. Rev. A* **1976**, *14*, 2071.

(33) Aguilar, J.; Combes, J.-M. *Commun. Math. Phys.* **1971**, *22*, 269–279.

(34) Balslev, E.; Combes, J.-M. *Commun. Math. Phys.* **1971**, *22*, 280–294.

(35) Simon, B. *Commun. Math. Phys.* **1972**, *27*, 1–9.

(36) Lipkin, N.; Moiseyev, N.; Brändas, E. *Phys. Rev. A* **1989**, *40*, 549.

(37) McCurdy Jr, C.; Rescigno, T. *Phys. Rev. Lett.* **1978**, *41*, 1364.

(38) Jolicard, G.; Austin, E. J. *Chem. Phys. Lett.* **1985**, *121*, 106–110.

(39) Jolicard, G.; Austin, E. J. *Chem. Phys.* **1986**, *103*, 295–302.

(40) Riss, U.; Meyer, H.-D. *J Phys. B: At. Mol. Opt. Phys.* **1993**, *26*, 4503.

(41) Riss, U.; Meyer, H.-D. *J Phys. B: At. Mol. Opt. Phys.* **1995**, *28*, 1475.

(42) Moiseyev, N; Hirschfelder, J. *J. Chem. Phys.* **1988**, *88*, 1063–1065.

(43) Kalita, D. J.; Gupta, A. K. *J. Chem. Phys.* **2011**, *134*, 094301.

(44) Sajeev, Y *Chem. Phys. Lett.* **2013**, *587*, 105–112.

(45) Rescigno, T.; McCurdy Jr, C.; Orel, A. E. *Phys. Rev. A* **1978**, *17*, 1931.

(46) Mishra, M.; Öhrn, Y.; Froelich, P. *Phys. Lett. A* **1981**, *84*, 4–8.

(47) Mishra, M.; Froelich, P.; Öhrn, Y. *Chem. Phys. Lett.* **1981**, *81*, 339–346.

(48) Samanta, K.; Yeager, D. L. *J. Phys. Chem. B* **2008**, *112*, 16214–16219.

(49) Samanta, K.; Yeager, D. L. *Int. J. Quantum Chem.* **2010**, *110*, 798–812.

(50) Whitenack, D. L.; Wasserman, A. *Phys. Rev. Lett.* **2011**, *107*, 163002.

(51) Sajeev, Y; Moiseyev, N. *J. Chem. Phys.* **2007**, *127*, 034105.

(52) Moiseyev, N.; Corcoran, C. *Phys. Rev. A* **1979**, *20*, 814.

(53) Medikeri, M. N.; Mishra, M. K. *Int. J. Quantum Chem.* **1994**, *52*, 29–37.

(54) Medikeri, M. N.; Mishra, M. K. *J. Chem. Phys.* **1995**, *103*, 676–682.

(55) Mahalakshmi, S; Mishra, M. K. *Chem. Phys. Lett.* **1998**, *296*, 43–50.

(56) Venkatnathan, A.; Mishra, M. K. *Chem. Phys. Lett.* **1998**, *296*, 223–232.

(57) Mahalakshmi, S; Mishra, M. K. *Indian J. Chem.* **2000**, *39A*, 22–31.

(58) Mahalakshmi, S; Venkatnathan, A.; Mishra, M. K. *J. Chem. Phys.* **2001**, *115*, 4549–4557.

(59) Samanta, K.; Tsogbayar, T.; Zhang, S. B.; Yeager, D. L. In *Adv. Quantum Chem.* Elsevier: 2018; Vol. 77, pp 317–390.

(60) Simon, B. *Phys. Lett. A* **1979**, *71*, 211–214.

(61) McCurdy, C. W.; Lauderdale, J. G.; Mowrey, R. C. *J. Chem. Phys.* **1981**, *75*, 1835–1842.

(62) Lauderdale, J. G.; McCurdy, C. W.; Hazi, A. U. *J. Chem. Phys.* **1983**, *79*, 2200–2205.

(63) Honigmann, M.; Buenker, R. J.; Liebermann, H.-P. *J. Chem. Phys.* **2006**, *125*.

(64) Honigmann, M.; Buenker, R. J.; Liebermann, H.-P. *J. Chem. Phys.* **2009**, *131*.

(65) Honigmann, M.; Buenker, R. J.; Liebermann, H.-P. *J. Comput. Chem.* **2012**, *33*, 355–362.

(66) White, A. F.; Epifanovsky, E.; McCurdy, C. W.; Head-Gordon, M. *J. Chem. Phys.* **2017**, *146*, 234107.

(67) Rom, N.; Lipkin, N.; Moiseyev, N. *Chem. Phys.* **1991**, *151*, 199–204.

(68) Karlsson, H. O. *J. Chem. Phys.* **1998**, *109*, 9366–9371.

(69) Sommerfeld, T; Riss, U.; Meyer, H.; Cederbaum, L.; Engels, B; Suter, H. *J. Phys. B: At. Mol. Opt. Phys.* **1998**, *31*, 4107.

(70) Santra, R.; Cederbaum, L. S. *J. Chem. Phys.* **2002**, *117*, 5511–5521.

(71) Feuerbacher, S.; Sommerfeld, T.; Santra, R.; Cederbaum, L. S. *J. Chem. Phys.* **2003**, *118*, 6188–6199.

(72) Sajeev, Y; Santra, R.; Pal, S. *J. Chem. Phys.* **2005**, *122*, 234320.

(73) Ghosh, A.; Vaval, N.; Pal, S. *J. Chem. Phys.* **2012**, *136*.

(74) Zuev, D.; Jagau, T.-C.; Bravaya, K. B.; Epifanovsky, E.; Shao, Y.; Sundstrom, E.; Head-Gordon, M.; Krylov, A. I. *J. Chem. Phys.* **2014**, *141*, 024102.

(75) Jagau, T.-C.; Zuev, D.; Bravaya, K. B.; Epifanovsky, E.; Krylov, A. I. *J. Phys. Chem. Lett.* **2014**, *5*, 310–315.

(76) Landau, A.; Moiseyev, N. *J. Chem. Phys.* **2016**, *145*, 164111.

(77) Ehara, M.; Kanazawa, Y.; Sommerfeld, T. *Chem. Phys.* **2017**, *482*, 169–177.

(78) Jagau, T.-C.; Bravaya, K. B.; Krylov, A. I. *Annu. Rev. Phys. Chem.* **2017**, *68*, 525–553.

(79) Das, S.; Sajeev, Y; Samanta, K. *J. Chem. Theory Comput.* **2020**, *16*, 5024–5034.

(80) Dempwolff, A. L.; Belogolova, A. M.; Sommerfeld, T.; Trofimov, A. B.; Dreuw, A. *J. Chem. Phys.* **2021**, *155*.

(81) Thodika, M.; Matsika, S. *J. Chem. Theory Comput.* **2022**, *18*, 3377–3390.

(82) Das, S.; Samanta, K. *J. Chem. Phys.* **2022**, *156*.

(83) Das, S.; Samanta, K. *Chem. Phys.* **2023**, *564*, 111712.

(84) Manolopoulos, D. E. *J. Chem. Phys.* **2002**, *117*, 9552–9559.

(85) Rom, N.; Engdahl, E.; Moiseyev, N. *J. Chem. Phys.* **1990**, *93*, 3413–3419.

(86) Elander, N.; Yarevsky, E. *Phys. Rev. A* **1998**, *57*, 3119.

(87) Telnov, D. A.; Chu, S.-I. *Phys. Rev. A* **1999**, *59*, 2864.

(88) Sajeev, Y; Sindelka, M.; Moiseyev, N. *Chem. Phys.* **2006**, *329*, 307–312.

(89) Kalita, D. J.; Gupta, A. K. *J. Chem. Phys.* **2010**, *133*, 134303.

(90) Riss, U.; Meyer, H. *J. Phys. B: At. Mol. Opt. Phys.* **1998**, *31*, 2279.

(91) Nissen, A.; Kreiss, G. *Commun. Comput. Phys.* **2011**, *9*, 147–179.

(92) Berenger, J.-P. *J. Comput. Phys.* **1994**, *114*, 185–200.

(93) Kalita, D. J.; Gupta, A. K. *J. Chem. Phys.* **2013**, *138*, 074313.

(94) Linderberg, J.; Öhrn, Y., *Propagators in Quantum Chemistry*; John Wiley & Sons: 2004.

(95) Medikeri, M. N.; Mishra, M. K. *Chem. Phys. Lett.* **1995**, *246*, 26–32.

(96) Moiseyev, N. *J. Phys. B: At. Mol. Opt. Phys.* **1998**, *31*, 1431.

(97) Bar-On, I.; Ryaboy, V. *SIAM J. Sci. Comput.* **1997**, *18*, 1412–1435.

(98) Kalita, D. J.; Gupta, A. K. *J. Chem. Phys.* **2012**, *137*.

(99) Szabo, A.; Ostlund, N. S., *Modern Quantum Chemistry: Introduction to Advanced Electronic Structure Theory*; Courier Corporation: 2012.

(100) Mishra, M.; Goscinski, O.; Öhrn, Y. *J. Chem. Phys.* **1983**, *79*, 5505–5511.

(101) Mishra, M.; Kurtz, H. A.; Goscinski, O.; Öhrn, Y. *J. Chem. Phys.* **1983**, *79*, 1896–1902.

(102) Venkatnathan, A.; Mahalakshmi, S; Mishra, M. K. *J. Chem. Phys.* **2001**, *114*, 35–47.

(103) Mishra, M.; Goscinski, O.; Öhrn, Y. *J. Chem. Phys.* **1983**, *79*, 5494–5504.

(104) Moiseyev, N.; Friedland, S.; Certain, P. R. *J. Chem. Phys.* **1981**, *74*, 4739–4740.

(105) Gamow, G. *Z. Phys.* **1928**, *51*, 204–212.

(106) Sajeev, Y; Mishra, M. K.; Vaval, N.; Pal, S. *J. Chem. Phys.* **2004**, *120*, 67–72.

(107) Yabushita, S.; McCurdy, C. W. *J. Chem. Phys.* **1985**, *83*, 3547–3559.

(108) Honigmann, M.; Hirsch, G.; Buenker, R. J.; Petsalakis, I. D.; Theodorakopoulos, G. *Chem. Phys. Lett.* **1999**, *305*, 465–473.

(109) McCurdy, C. W.; Rescigno, T. N.; Davidson, E. R.; Lauderdale, J. G. *J. Chem. Phys.* **1980**, *73*, 3268–3273.

(110) Berman, M.; Estrada, H.; Cederbaum, L. S.; Domcke, W. *Phys. Rev. A* **1983**, *28*, 1363.

(111) Schneider, B. I.; Collins, L. A. *Phys. Rev. A* **1984**, *30*, 95.

(112) Schneider, B.; Le Dourneuf, M; Lan, V. K. *Phys. Rev. Lett.* **1979**, *43*, 1926.

(113) Chao, J.-Y.; Falcetta, M.; Jordan, K. *J. Chem. Phys.* **1990**, *93*, 1125–1135.

(114) Dubé, L; Herzenberg, A *Phys. Rev. A* **1979**, *20*, 194.

(115) Rescigno, T.; Orel, A.; McCurdy, C. *J. Chem. Phys.* **1980**, *73*, 6347–6348.

(116) Donnelly, R. A. *Int. J. Quantum Chem.* **1982**, *22*, 653–659.

(117) Belogolova, A.; Dempwolff, A.; Dreuw, A; Trofimov, A. *J. Phys.: Conf. Ser.* **2021**, *1847*, 012050.

(118) Ehrhardt, H; Langhans, L; Linder, F; Taylor, H. *Phys. Rev.* **1968**, *173*, 222.

(119) Zubek, M.; Szmytkowski, C. *J. Phys. B: At. Mol. Phys. (1968-1987)* **1977**, *10*, L27.

(120) Chandra, N *Phys. Rev. A* **1977**, *16*, 80.

(121) Donnelly, R. A. *Int. J. Quantum Chem.* **1985**, *28*, 363–368.

(122) Mishra, M. K.; Medikeri, M. N.; Venkatnathan, A.; Mahalakshmi, S *Mol. Phys.* **1998**, *94*, 127–138.

(123) Mishra, M. K.; Medikeri, M. N. In *Adv. Quantum Chem.* Elsevier: 1996; Vol. 27, pp 223–295.

(124) Bisgaard, P; Bruch, R; Dahl, P; Fastrup, B; Rødbro, M *Phys. Scr.* **1978**, *17*, 49.

(125) Rodbro, M; Bruch, R.; Bisgaard, P *J. Phys. B: Atom. Mol. Phys.* **1979**, *12*, 2413.

(126) Kelly, H. P. *Phys. Rev. A* **1974**, *9*, 1582.

(127) Palmquist, M; Altick, P.; Richter, J; Winkler, P; Yaris, R *Phys. Rev. A* **1981**, *23*, 1795.

(128) Kurtz, H.; Jordan, K. D. *J. Phys. B: Atom. Mol. Phys.* **1981**, *14*, 4361.

(129) Krylstedt, P; Rittby, M; Elander, N; Brandas, E *J. Phys. B: Atom. Mol. Phys.* **1987**, *20*, 1295.

(130) McNutt, J. F.; McCurdy, C. W. *Phys. Rev. A* **1983**, *27*, 132.

(131) Samanta, K.; Yeager, D. L. *J. Phys. Chem. B* **2008**, *112*, 16214–16219.

(132) Tsednee, T.; Liang, L.; Yeager, D. L. *Phys. Rev. A* **2015**, *91*, 022506.

(133) Tsogbayar, T.; Yeager, D. L. *Chem. Phys.* **2017**, *482*, 201–207.

(134) Falcetta, M. F.; Reilly, N. D.; Jordan, K. D. *Chem. Phys.* **2017**, *482*, 239–243.

(135) Venkatnathan, A.; Mishra, M. K.; Jensen, H. J. A. *Theor. Chem. Acc.* **2000**, *104*, 445–454.

(136) Huzinaga, S. *J. Chem. Phys.* **1965**, *42*, 1293–1302.

(137) Kurtz, H. A.; Öhrn, Y. *Phys. Rev. A* **1979**, *19*, 43.

(138) Reinhardt, W. P. *Ann. Rev. Phys. Chem.* **1982**, *33*, 223–255.

(139) Woon, D. E.; Dunning Jr, T. H. *J. Chem. Phys.* **1995**, *103*, 4572–4585.

(140) Dance, D.; Walker, I. C. *Chem. Phys. Lett.* **1973**, *18*, 601–603.

(141) Van Veen, E.; Plantenga, F. *Chem. Phys. Lett.* **1976**, *38*, 493–497.

(142) Kochem, K.-H.; Sohn, W; Jung, K; Ehrhardt, H; Chang, E. *J. Phys. B: Atom. Mol. Phys.* **1985**, *18*, 1253.

(143) Dressler, R; Allan, M *J. Chem. Phys.* **1987**, *87*, 4510–4518.

(144) Andric, L; Hall, R. *J. Phys. B: At. Mol. Opt. Phys.* **1988**, *21*, 355.

(145) May, O.; Fedor, J.; Ibănescu, B. C.; Allan, M. *Phys. Rev. A* **2008**, *77*, 040701.

(146) Krumbach, V; Nestmann, B.; Peyerimhoff, S. *J. Phys. B: At. Mol. Opt. Phys.* **1989**, *22*, 4001.

Appendix A

Supporting Information for Chapter 3.

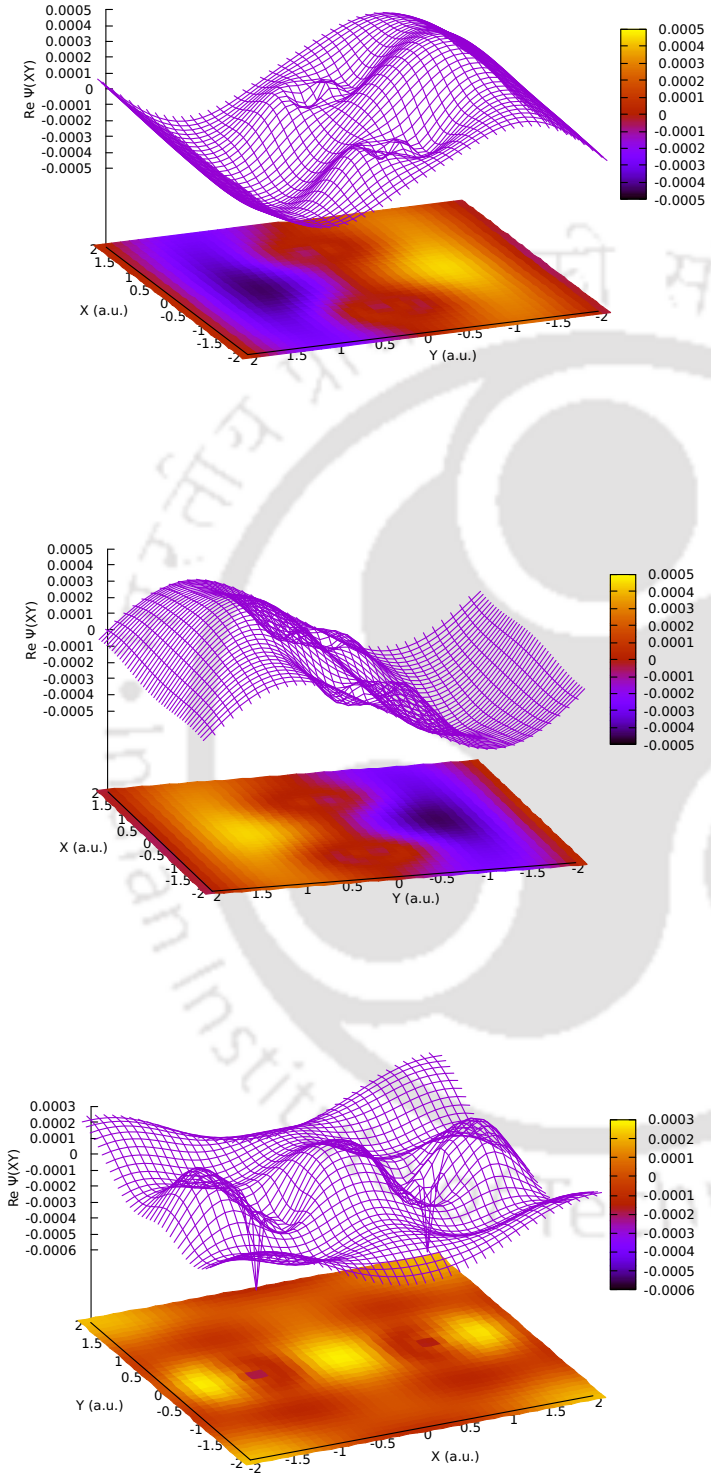

FIGURE A1: Wavefunctions of artifacts shown in θ_0-trajectories of orbital energies of N_2

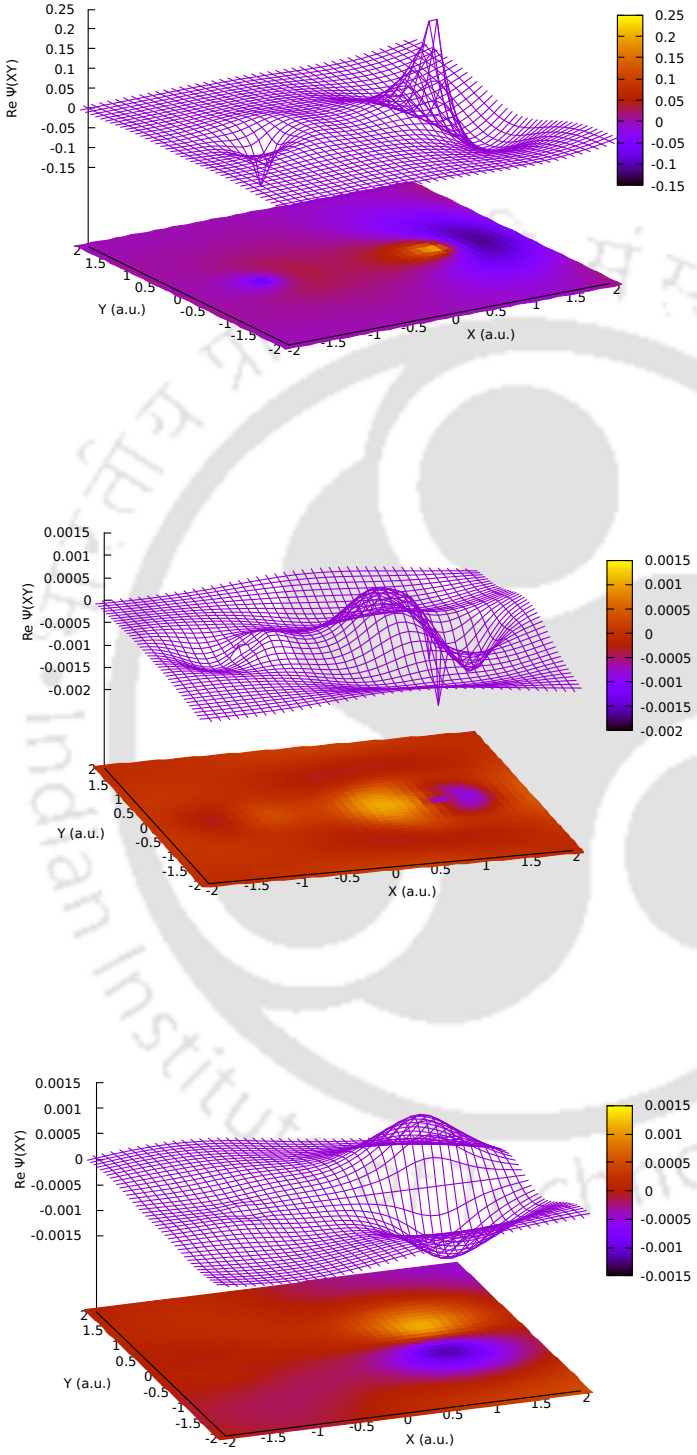

FIGURE A2: Wavefunctions of artifacts shown in θ_0-trajectories of orbital energies of CO

List of Publications

Articles Published in International/National Journals

1. Banuary, M., Gupta, A.K., Application of Modified Smooth Exterior Scaling Method to Study $^2\Pi_g$ N_2^- and $^2\Pi$ CO^- Shape Resonances. *ACS Omega* 8(7), 7143–7150 (2023).

2. Banuary, M., Kumar, D., Gupta, A.K., Use of dilated electron propagator in conjunction with modified smooth exterior scaling method to characterize ^{2}S Be^+ ($1s^{-1}$), ^{2}S Ne^+ ($1s^{-1}$) Auger and ^2P Be^- shape resonances. (Accepted for Publication)

3. Banuary, M., Kumar, D., Gupta, A.K., Study of Effects of Diffused Basis Functions in Characterizing Electron Molecule Scattering Shape Resonances Using Modified Smooth Exterior Scaling. (To be submitted)

Presentations and Proceedings in International/National Conferences

1. Oral Presentation in Advances in Sustainable Chemistry and Material Science 2022, Bodoland University, India.

2. Poster Presentation in Theoretical Chemistry Symposium 2023, IIT Madras, India.